Defence Research and Development Canada
Recherche et développement pour la défense Canada

DEFENCE R&D DÉFENSE

Separation of target rigid body and micro-Doppler effects in ISAR/SAR imaging

T. Thayaparan

Defence R&D Canada – Ottawa
TECHNICAL MEMORANDUM
DRDC Ottawa TM 2006-187
September 2006

Canada

Separation of target rigid body and micro-Doppler effects in ISAR/SAR imaging

T. Thayaparan
Defence R&D Canada – Ottawa

Defence R&D Canada – Ottawa

Technical Memorandum

DRDC Ottawa TM 2006-187

September 2006

Abstract

The micro-Doppler (m-D) effect is caused by moving parts of the radar target. This effect can degrade the quality of the ISAR/SAR image. However, at the same time, it carries information about the features of moving parts. The separation of the patterns caused by the stationary parts of the target from those caused by the moving (rotating or vibrating) parts is the topic of this report. Two techniques for the separation of the rigid part from the rotating parts have been proposed. The first technique is based on the time-frequency (TF) representation with sliding windows and order statistics techniques. The first step in this technique is the recognition of rigid parts in the range/cross-range plane. In the second step, the spectrogram and order statistics setup are employed to obtain the signals caused by the moving parts. The second technique based on the Radon transform can be applied in the case of very emphatic m-D effect. In the first step the rotating parts are recognized, based on the inverse Radon transform. After masking these patterns, a radar image with the rigid body reflection can be obtained. The proposed methods are illustrated by examples. The proposed methods not only focus the distorted SAR/ISAR images, but also provide additional information about the rotating/vibrating features of the target.

Résumé

L'effet micro-Doppler (m-D) est causé par les parties mobiles d'une cible radar. Il peut dégrader l'image ISAR/SAR. Toutefois, il est également porteur d'information sur les caractéristiques de ces parties mobiles. La séparation des formes dues respectivement aux parties fixes et aux parties mobiles (tournantes ou vibrantes) de la cible est l'objet du présent rapport. Deux techniques ont été proposées pour séparer ces deux types de formes. L'une utilise la représentation temps-fréquence (TF) avec fenêtres mobiles et statistiques d'ordre. Elle permet d'abord de reconnaître les parties rigides dans le plan site/azimut. Dans un deuxième temps, le spectrogramme et la configuration des statistiques d'ordre sont employés pour obtenir les signaux dus aux parties mobiles. La deuxième technique, basée sur la transformée de Radon, peut être appliquée dans le cas d'effets m-D très marqués. Les parties tournantes sont d'abord reconnues, à l'aide de la transformée de Radon inverse. Après masquage de ces formes, on peut obtenir une image radar du corps rigide. Des exemples illustrent les méthodes proposées, qui non seulement permettent de mettre au point les images SAR/ISAR déformées, mais fournissent une information supplémentaire sur les parties tournantes/vibrantes de la cible.

This page intentionally left blank.

Executive summary

If a target or any structure on a target has mechanical vibration or rotation in addition to its bulk translation, it might induce a frequency modulation on the returned signal that generates sidebands about the target's Doppler frequency shift. This is called the micro-Doppler effect. Radar signals returned from a target that incorporates vibrating or rotating structures, such as propellers of a fixed-wing aircraft, rotors of a helicopter, or the engine compressor and blade assemblies of a jet aircraft, contain micro-Doppler characteristics related to these structures. The micro-Doppler effect enables us to determine the dynamic properties of the target and it offers a new approach for the analysis of target signatures. Micro-Doppler features serve as additional features that are complementary to those made available by existing methods. The micro-Doppler effect can be used to identify specific types of vehicle, and determine their movement and the speed of their engines. Vibrations generated by a vehicle engine can be detected by radar signals returned from the surface of the vehicle. From micro-Doppler modulations in the engine vibration signal, one can distinguish whether it is a gas turbine engine of a tank or the diesel engine of a bus.

Micro-Doppler effect appears in the SAR/ISAR image of a target whenever the target has one or more rotating or vibrating parts. If the frequency modulations on the returned signal caused by the moving parts are not filtered, then the micro-Doppler effect can introduce distortion in the SAR/ISAR images. The observation of very large distortions from experimental SAR/ISAR data has been reported. On the other hand, the micro-Doppler effect also carries information about the features of moving parts of a target that are complementary to existing target recognition methods. This report proposes two techniques for the separation of rigid body radar image from micro-Doppler effect caused signal in SAR/ISAR imaging. The first technique is based on the order statistics of the spectrogram samples. In order to separate the patterns caused by the rotating and rigid body parts, the spectrogram is evaluated for various window sizes. The spectrogram evaluated with a narrow window produces a high concentration of the signal caused by rotating parts, while the spectrogram evaluated for a wide window produces a high concentration of the signal corresponding to the rigid body parts. The second technique is based on the Radon transform processing of the radar signals. It can be useful in the case of radar targets with a dominant micro-Doppler signals. Both proposed methods have shown satisfactory accuracy for the considered complex simulated examples, including rotating and vibrating target parts.

The proposed method not only can focus distorted SAR/ISAR images, but also can provide additional information about the rotating/vibrating features of the target. Therefore, new algorithms and methods will have to be further investigated to sep-

arate the stationary and non-stationary components of the target of interest.

T. Thayaparan; 2006; Separation of target rigid body and micro-Doppler effects in ISAR/SAR imaging; DRDC Ottawa TM 2006-187; Defence R&D Canada – Ottawa.

Sommaire

Lorsqu'une cible ou une structure d'une cible présente une vibration ou rotation mécanique en plus d'une translation globale, elle peut induire une modulation de la fréquence du signal réfléchi, ce qui produit des bandes latérales de part et d'autre du déplacement de fréquence Doppler de la cible. On parle alors d'effet micro-Doppler. Les signaux radar réfléchis par une cible comportant des structures vibrantes ou tournantes, par exemple hélices d'aéronef à voilure fixe, rotors d'hélicoptères ou ensembles compresseur-aubes d'avions à réaction, présentent des caractéristiques micro-Doppler associées à ces structures. L'effet micro-Doppler permet de déterminer les propriétés dynamiques de la cible et offre une nouvelle approche pour l'analyse de signatures de cibles. Ces caractéristiques complètent celles que fournissent les méthodes existantes. L'effet micro-Doppler peut servir à identifier des types particuliers de véhicules et à déterminer leur mouvement et la vitesse de leurs moteurs. Les vibrations produites par le moteur d'un véhicule peuvent être détectées par des signaux radars réfléchis à la surface du véhicule. À partir de modulations micro-Doppler du signal de vibration du moteur, on peut distinguer s'il s'agit du moteur à turbine à gaz d'un tank ou du moteur diesel d'un autobus.

L'effet micro-Doppler apparaît dans l'image SAR/ISAR d'une cible lorsque celle-ci comporte une ou plusieurs parties tournantes ou vibrantes. Si les modulations de fréquence du signal réfléchi dues aux parties mobiles ne sont pas filtrées, l'effet micro Doppler peut déformer les images SAR/ISAR. On a observé des déformations très importantes de données SAR/ISAR expérimentales. Par contre, l'effet micro-Doppler fournit aussi de l'information sur les caractéristiques des parties mobiles d'une cible qui complète l'information provenant des méthodes de reconnaissance de cibles existantes. Le présent rapport propose deux techniques pour séparer l'image radar du corps rigide et le signal dû à l'effet micro-Doppler dans l'imagerie SAR/ISAR. La première se fonde sur les statistiques d'ordre d'échantillons de spectrogramme. Pour séparer les formes dues aux parties tournantes et aux parties rigides, le spectrogramme est évalué avec diverses tailles de fenêtres, une fenêtre étroite produisant une forte concentration du signal due aux parties tournantes, et une fenêtre large une forte concentration du signal correspondant aux parties du corps rigide. La deuxième technique se fonde sur le traitement des signaux radar par la transformée de Radon. Elle peut être utile dans le cas de cibles radar avec signal micro-Doppler dominant. Les deux méthodes proposées ont montré une exactitude satisfaisante dans les cas de simulation complexe étudiés, comprenant des parties de cible tournantes et vibrantes.

La méthode proposée peut non seulement mettre au point les images SAR/ISAR déformées, mais aussi fournir une information supplémentaire sur les parties tournantes et vibrantes de la cible. De nouveaux algorithmes et méthodes devront donc

être étudiés plus en profondeur afin de séparer les composantes fixes et mobiles de la cible d'intérêt.

T. Thayaparan; 2006; Separation of target rigid body and micro-Doppler effects in ISAR/SAR imaging; DRDC Ottawa TM 2006-187; R & D pour la défense Canada – Ottawa.

Table of contents

List of figures

1 Introduction

Micro-Doppler (m-D) effects appear in the SAR/ISAR image when the target has one or more rotating or vibrating parts. This effect can degrade the quality of the radar image. However, the m-D effect, at the same time, carries information about the features of moving parts (type, velocity, size, etc.). Several papers have been written about the ways to deal with the m-D effect. The wavelet analysis of the helicopter and human data, along with the time-frequency (TF) representation based imaging system, is presented in [1, 2, 3]. Details on the physics of the m-D effect, with some typical examples, are given in [4, 5, 6, 7]. A method for separating the m-D effect from the radar image, based on the chirplet transform, is proposed in [8, 6]. The part of the radar signal, obtained as a result of the m-D effect, after appropriate separation from the rest of the radar target image, can be used for estimating the rotating part parameters. In [8, 6], the received signal has been expanded into a set of chirplet functions. The obtained chirplet functions are divided into two groups: the chirplets with the small chirp-rate parameter (associated to the rigid part) and the chirplets with the large chirp-rate parameter (associated to the moving parts). The calculation burden of this procedure is high, since the chirplet dictionary could be extremely large. Both wavelet-based and chirplet based procedures are used in [9, 6] to extract the m-D features such as the rotating frequency of the antenna from SAR data. The analysis of the TF representation application in radar target identification is presented in [10]. The reduced interference distributions from the Cohen class are applied as a tool for the target identification. A technique for the m-D effect estimation from the reflected signal, based on the TF signatures and decomposition of basis functions, is presented in [11]. This technique can be used for m-D effect signals that can be represented as sinusoidal FM signals.

In this report, two procedures for the separation of signals coming from the rigid (slowly moving) body and rotating parts are proposed. In order to analyze the m-D effect, we will perform TF (more accurately space/spatial-frequency) analysis using a sliding window. Based on the order statistics of the obtained TF representations, we will make decisions on whether the components belong to the rigid body or to the rotating target parts [21]. The other approach is based on the Radon transform (RT). The TF representation of the sinusoidal FM signal can be concentrated in a single point by applying the inverse RT to the TF representation. In this way, the patterns of the rotating parts can be easily extracted from the target signal [21].

The report is organized as follows. ISAR signal modeling is described in Section 2, modeling signals from both the rigid body and the moving parts of the target. The method for separation of the rigid body and the moving elements from the radar image, based on the order statistics of the TF representation with a sliding window, is given in Section 3. The separation of rotating patterns from the radar image using

the inverse RT is presented in Section 4. The simulation study is given in Section 5. The concluding remarks with possible directions for the further research are given in Section 6. Annex A provides the basic procedure of the order statistics estimations.

2 Radar Signal Model

Consider a radar signal consisting of M continuous wave coherent pulses:

$$v_M(t) = \sum_{m=0}^{M-1} v_0(t - mT_r), \tag{1}$$

where $v_0(t)$ is the basic impulse limited within the interval $-T_r/2 \leq t < T_r/2$. The linear frequency modulated (FM) signal is used in our simulations as a basic impulse: $v_0(t) = \exp(j\pi Bt^2/T_r)$, where B is the bandwidth control parameter while T_r is the pulse repetition time. The alternative radar model used in practice has radar pulses with stepped frequencies, however, this model is not studied in this report. The defocusing effect considered in this report and time-frequency (TF) signatures of the obtained radar signals have similar behavior for these two forms of radar signals [19, 20].

The signal emitted toward the radar target can be written as:

$$u(t) = e^{j2\pi f_0 t} v_M(t), \tag{2}$$

where f_0 is the radar operating frequency. The received signal, reflected from a single reflector target at distance $d(t)$, is delayed for $2d(t)/c$, with σ being the reflection coefficient and c being the propagation rate:

$$u_R(t) = \sigma u\left(t - 2d(t)/c\right). \tag{3}$$

The demodulation of the received signal can be performed by multiplying the received with the transmitted signal $u(t)$:

$$q(t) = \sigma u^*(t - 2d(t)/c)u(t) =$$

$$\sigma \exp(j4\pi f_0 d(t)/c) \sum_{m=0}^{M-1} v_0^*(t - 2d(t)/c - mT_r) \sum_{m=0}^{M-1} v_0(t - mT_r - T_0). \tag{4}$$

The parameter T_0 is used in radar imaging for compensation of target distance. For properly selected T_0 and after highpass filtering, the signal $q(t)$ can be approximately written as:

$$q(t) \approx \sigma \exp(j4\pi f_0 d(t)/c) \sum_{m=0}^{M-1} v_0^*(t - 2d(t)/c - mT_r) v_0(t - mT_r) = \sum_{m=0}^{M-1} q(m,t), \tag{5}$$

where

$$\begin{aligned} q(m,t) &= \sigma \exp(j4\pi f_0 d(t)/c) v_0^*(t - 2d(t)/c - mT_r) v_0(t - mT_r), \\ & t \in [(m - 1/2)T_r, (m + 1/2)T_r), \\ &= \sigma \exp(j4\pi f_0 d(t)/c) \exp(j4\pi B d(t)(t - mT_r)/(cT_r)) \exp(-j\pi B(2d(t)/c)^2/T_r). \end{aligned} \tag{6}$$

Keeping in mind that $B \ll f_0$, we can neglect $\exp(-j\pi B(2d(t)/c)^2/T_r)$ with respect to the other two components. The value of $q(m,t)$ can approximately be written as:

$$q(m,t) \approx \sigma \exp(j4\pi f_0 d(t)/c) \exp(j4\pi B d(t)(t - mT_r)/(cT_r)). \tag{7}$$

This signal is commonly given in the form:

$$q(m,\tau) \approx \sigma \exp(j4\pi f_0 d(\tau + mT_r)/c) \exp(j4\pi B d(\tau + mT_r)\tau/(cT_r)), \tag{8}$$

where $t = \tau + mT_r$. Parameter $\tau \in [-T_r/2, T_r/2)$ is referred to as fast-time, while $m = 0, 1, ..., M-1$, is called the slow-time coordinate. Commonly, in actual radar systems, signals are discretized in the fast-time coordinate with sampling rate $T_s = T_r/N$, $\tau = nT_s$, where $n \in [-N/2, N/2)$. The classical radar setup assumes that the radar target position is a linear function of time $d(t) = D_0 + Vt$. Then the radar model produces:

$$q(m,\tau) \approx \sigma \exp(j4\pi f_0 D_0/c) \exp(j4\pi V m f_0 T_r/c) \exp(j4\pi \tau B D_0/(cT_r)). \tag{9}$$

A two-dimensional (2D) FT of this signal over m and τ is approximately:

$$Q(\omega_\tau, \omega_m) = \int_\tau \sum_{m=0}^{M-1} q(m,\tau) e^{-j\omega_\tau \tau - j\omega_m m} d\tau \approx$$

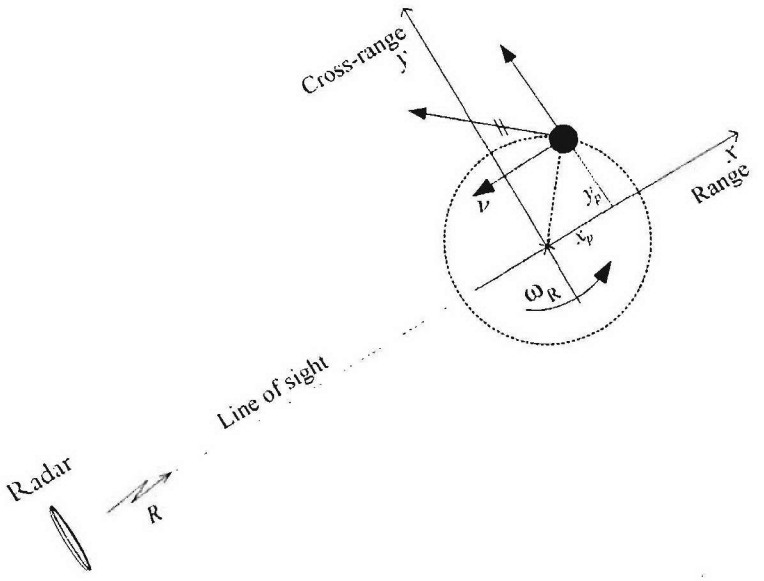

Figure 1: *Illustration of the radar target geometry.*

$$\int_\tau \sum_{m=0}^{M-1} \sigma \exp(j4\pi f_0 D_0/c) \exp(j4\pi V m f_0 T_r/c) \exp(j4\pi\tau B D_0/(cT_r)) e^{-j\omega_\tau \tau - j\omega_m m} d\tau$$

$$= \sigma \exp(j4\pi f_0 D_0/c) \int_\tau \exp(j4\pi\tau B D_0/(cT_r)) e^{-j\omega_\tau \tau} d\tau \sum_{m=0}^{M-1} \exp(j4\pi V m f_0 T_r/c) e^{-j\omega_m m}$$

$$= (2\pi)\sigma \exp(j4\pi f_0 D_0/c)\delta(\omega_\tau - 4\pi B D_0/(cT_r)) \frac{\sin((\omega_m - 4\pi V f_0 T_r/c)M/2)}{\sin((\omega_m - 4\pi V f_0 T_r/c)/2)}$$

$$\times e^{-j(\omega_m - 4\pi V f_0 T_r/c)(M-1)/2}. \tag{10}$$

$$|Q(\omega_\tau, \omega_m)| = |(2\pi)\sigma \exp(j4\pi f_0 D_0/c)\delta(\omega_\tau - 4\pi B D_0/(cT_r))$$
$$\times \frac{\sin((\omega_m - 4\pi V f_0 T_r/c)M/2)}{\sin((\omega_m - 4\pi V f_0 T_r/c)/2)} e^{-j(\omega_m - 4\pi V f_0 T_r/c)(M-1)/2}$$

$$= |2\pi||\sigma|| \exp(j4\pi f_0 D_0/c)||\delta(\omega_\tau - 4\pi B D_0/(cT_r))| \left| \frac{\sin((\omega_m - 4\pi V f_0 T_r/c)M/2)}{\sin((\omega_m - 4\pi V f_0 T_r/c)/2)} \right| |$$
$$\times |e^{-j(\omega_m - 4\pi V f_0 T_r/c)(M-1)/2}| \tag{11}$$
$$= |(2\pi)\sigma\delta(\omega_\tau - 4\pi B D_0/(cT_r)) \frac{\sin((\omega_m - 4\pi V f_0 T_r/c)M/2)}{\sin((\omega_m - 4\pi V f_0 T_r/c)/2)}|$$

$$\approx (2\pi)\sigma\delta(\omega_\tau - 4\pi BD_0/(cT_r))M\delta(\omega_m - 4\pi V f_0 T_r/c)$$

since

$$\frac{\sin(\alpha M)}{\sin(\alpha)} \approx M\delta(\alpha)$$

for relatively large M.

Therefore, for large M we can write the magnitude of $Q(\omega_\tau, \omega_m)$ as:

$$|Q(\omega_\tau, \omega_m)| \approx (2\pi)\sigma\delta(\omega_\tau - 4\pi BD_0/(cT_r))M\delta(\omega_m - 2V f_0 T_r/c). \quad (12)$$

The distance can be approximately written as $d(t) \approx R(t) + x_p\cos(\theta(t)) + y_p\sin(\theta(t))$, where $R(t)$ is the distance of the target rotation center from the radar, where coordinates of the scatterer, for $\tau = 0$, are (x_p, y_p) (see Figure 1). The coordinate system is formed in such a way that the coordinate x is the line of sight. Assume constant rotation velocity $\theta(t) = \omega_R t$, with relatively small angular movement of the target $|\omega_R T_r| \ll 1$ (it implies that $\cos(\theta(t)) \approx 1$ and $\sin(\theta(t)) \approx 0$). According to the introduced conditions $d(t) \approx x_p$ and $v(t) = d'(t) = -x_p\theta'(t)\sin(\theta(t)) + y_p\theta'(t)\cos(\theta(t)) \approx y_p\theta'(t)\cos(\theta(t)) \approx y_p\omega_R$. Commonly, it is assumed that $R(t)$ is compensated by adjusting T_0 in (4). Thus, we will not consider it in our algorithm. Then $|Q(\omega_\tau, \omega_m)|$ can be written as:

$$\begin{aligned} |Q(\omega_\tau, \omega_m)| &\approx (2\pi)\sigma M\delta(\omega_\tau - 4\pi Bx_p/(cT_r))\delta(\omega_m - 4\pi y_p\omega_R f_0 T_r/c) \\ &= (2\pi)\sigma M\delta(\omega_\tau - c_1 x_p)\delta(\omega_m - c_2 y_p). \end{aligned} \quad (13)$$

It represents the ISAR image of scatterer (x_p, y_p) for a given instance under introduced assumptions. Note that the constants that determine the resolution of the radar image are given by $c_1 = 4\pi B/(cT_r)$ and $c_2 = 4\pi\omega_R f_0 T_r/c$. The radar image is formed as superposition of radar images of all scatterers (x_p, y_p), $p = 1, 2, ..., P$. It is approximately given as:

$$|Q(\omega_\tau, \omega_m)| = \sum_{p=1}^{P}(2\pi)\sigma_p\delta(\omega_\tau - c_1 x_p)\delta(\omega_m - c_2 y_p), \quad (14)$$

where σ_p is the reflection coefficient that corresponds to the p-th scatterer point.

The common ISAR imaging model assumes that all the point-scatterers share the same angular motion. However, the radar target can have moving parts (rotating or vibrating). In this model, the received signal, within the m-th radar sweep, can be written as [8]:

$$q_m(t) = \sum_{p=1}^{P} \sigma_p \exp\left\{-j\frac{4\pi f_0}{c}[R_B(t) + x_p \cos\theta_B(t) + y_p \sin\theta_B(t)]\right\} +$$
$$\sigma_R \exp\left\{-j\frac{4\pi f_0}{c}[R_R(t) + x_R \cos\theta_R(t) + y_R \sin\theta_R(t)]\right\}, \qquad (15)$$

where σ_p is the reflection coefficient of the p-th scatterer, f is the radar operating frequency, (x_p, y_p) are coordinates of the scatterer point (x coordinate is in the direction of line-of-sight, according to Figure 1). The target translation and angular motion are denoted by $R(t)$ and $\theta(t)$, with indices B and R corresponding to the rigid body and rotating parts, respectively. Here we assume a single rotating point. In general, we will have a radar target with an arbitrary number of moving parts. The motion compensation techniques [8, 12] are employed to remove the influence of the translation motion. Thus, we can assume that $R_B(t) \to 0$ and $R_R(t) \to 0$. For the main body holds $|\theta_B(t)| \ll 1$. It results in $\cos\theta_B(t) \approx 1$ and $\sin\theta_B(t) \approx \theta_B(t) = \omega_B t$, where ω_B is the effective body rotation rate, after the motion compensation. This approximation cannot be applied to rotating parts since, $\theta_R(t)$ can vary rapidly. The received signal can now be written as:

$$q_m(t) = \sum_{p=1}^{P} \sigma_p \exp\left\{-j\frac{4\pi f_0}{c}[x_p + y_p \omega_B t]\right\}$$
$$+\sigma_R \exp\left\{-j\frac{4\pi f_0}{c}[x_R \cos\theta_R(t) + y_R \sin\theta_R(t)]\right\}. \qquad (16)$$

The first term in (16) represents sinusoids concentrated at frequencies proportional to y_p, $p \in [1, P]$. The information on other coordinates can be obtained based on processing of all returned radar signals. The radar image is commonly obtained by a 2D FT of the compressed received signal denoted as $q(m,t) \equiv q_m(t)$. The second term in (16) represents sinusoidally modulated FM signal caused by the rotating part with a relatively large $\theta_R(t)$ during the repetition interval. This signal can cover the large portion of the TF plane. It can mask a significant part of the radar image. The influence of the rotating and vibrating parts on the radar image is commonly referred to as the m-D effect. The detailed considerations of physics of this effect, mathematical derivations and simulation studies are given in [4, 5, 7]. This effect should be removed from the radar image of the rigid body part, but at the same time it contains important information related to the radar target. In the next section, a technique for the separation of the rigid body and rotating parts influence from the received signal is presented. It is based on the running window TF representation and the L-statistics. In Section 4 the RT is applied for removing influence of strong rotating parts.

3 Time-frequency analysis and order statistics approach

3.1 Basic idea

In order to explain the approach for separation of the m-D effect from the ISAR image, we will consider the experimental setup used in [8]. The target with five scatterers at positions: $(0,0)$, $(\pm 6,0)$ and $(0,\pm 6)$ is considered (positions are in meters). The reflection coefficient for the central point is 5, for the second pair of points is 1, while for the third pair is 2. The positions of the six scatterers are shown in Figure 2. Scatterer 6 rotates around scatterer 2 at a rate of 6.67 Hz and a rotation radius of 20 cm, with the reflection coefficient of 3.33. We assume that the radar has a centre frequency $f = 10$ GHz, bandwidth $B = 800$ MHz, and $PRF = 1400$ Hz. The target body rotates about 4^o over 384 pulses during the data collection time. Therefore the coherent integration time is $T_r = 0.2743$ s. The range and cross-range resolutions are $R_{range} = c/2B = 0.1874$ m and $R_{cross-range} = c/2f\omega_c T_c = 0.2149$ m, respectively.

For the analysis of the received signals $q(\tau, m)$ we will use the spectrogram (SPEC) as a TF tool:

$$SPEC(\tau, \omega_\tau; m) = \left| \int_{-\infty}^{\infty} q(\tau + \tau_w, m) w(\tau_w) e^{-j\omega_\tau \tau_w} d\tau_w \right|^2, \qquad (17)$$

where $w(\tau_w)$ is a window function. We will assume that the signal $q(\tau, m)$ is discretized, producing discretized $SPEC(n, \omega_\tau; m)$.

The SPEC for various window lengths exhibits different properties for various kinds of signals. The SPEC of the considered radar signal, for a narrow Hanning window with 32 samples, is shown in Figure 3a. The SPEC calculated with a wide Hanning window with 128 samples is depicted in Figure 3b. In both figures we can see the stationary patterns, caused by the rigid body, parallel to the time-axis. The SPEC of the rigid body parts is better concentrated for wider than for narrower windows. Also, a sinusoidal pattern caused by the rotating point can easily be seen. It is in accordance with the assumed model for these parts. However, the sinusoidal FM signal is better concentrated for the narrower window case.

This example clearly shows that the rigid body and rotating parts in the TF plane should be studied with the TF representation with various window lengths. Upper arrow in Figure 3a denotes the frequency where only the influence of the rotating parts exists. For that frequency relatively small number of TF samples assume high

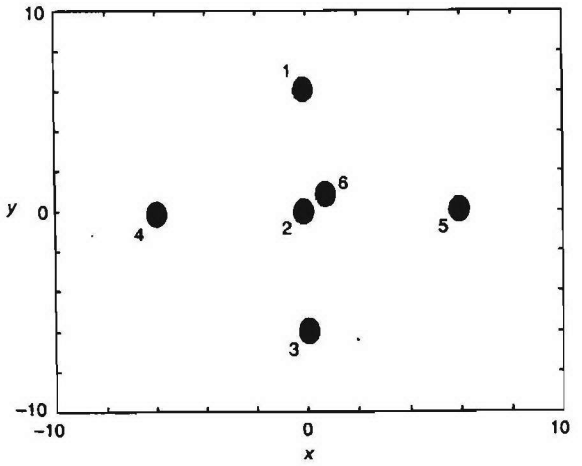

Figure 2: *Point-scatterer representation of the original target consisting of five rigid points (1-5) and one rotating point (6) with strengths 2, 5, 2, 1, 1, and 3.33, respectively.*

values. However, in the region of the signal caused by the rigid body (see lower arrow) all TF samples have high values.

For a narrow window in the SPEC we can see that the number of points belonging to the rotating parts is not high as compared to the considered interval. Therefore, we can consider the mean value of the smallest SPEC samples, as a good measure of the rigid body and rotating parts influence. In the region of the rigid body this measure will be high, since the rigid body has influence over the entire considered interval while the influence of the signal caused by rotating part will be removed.

3.2 L-statistics

For this kind of analysis a linear combination of order statistics (L-statistics) gives a powerful notational and analytic tool. The L-statistics of the SPEC samples can be defined as [13]:

$$L(\omega_\tau) = \sum_{n=0}^{N-1} a_n S_{(n)}(\omega_\tau; m) \tag{18}$$

where $S_{(n)}(\omega_\tau; m)$ are samples from the set $\mathbf{S}_{\omega_\tau,m} = \{SPEC(\tau, \omega_\tau; m), \tau \in [0, T_r)\}$, sorted into a non-decreasing sequence: $S_{(n)}(\omega_\tau; m) \leq S_{(n+1)}(\omega_\tau; m)$. In order to visualize how this measure can be used to distinguish signals caused by

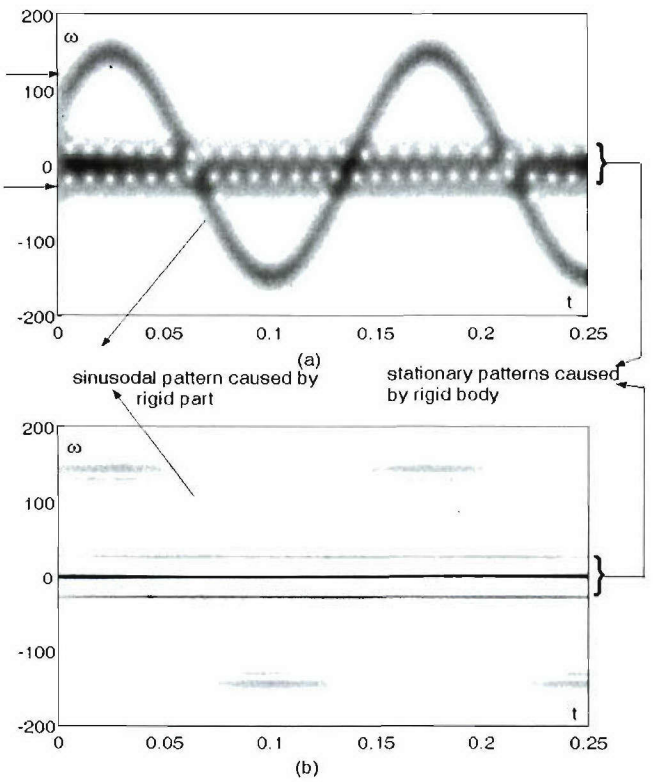

Figure 3: *Spectrogram of the radar signal reflected from the target with emphatic m-D effect calculated with: (a) Narrow window; (b) Wide window.*

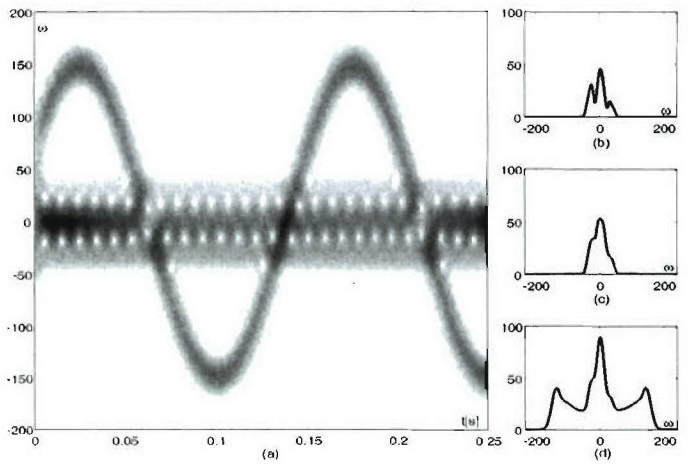

Figure 4: *TF representation and order statistics of the received signal: (a) Spectrogram; (b) $L_1(\omega_\tau)$; (c) $L_2(\omega_\tau)$; (d) $L_3(\omega_\tau)$. The x-axis corresponds to time and the y-axis corresponds to frequency.*

various parts of the radar target, we repeat Figure 4a. Three order statistics of this SPEC are presented on the right hand side of this figure (Figures 4b, c and d). They are calculated as:

- $a_n = 4/N$ for $n \in [0, N/4)$ and $a_n = 0$ elsewhere, i.e., for the smallest magnitude SPEC samples (statistics $L_1(\omega_\tau)$);
- $a_{N/2-1} = a_{N/2} = 1/2$ and $a_n = 0$ elsewhere, i.e., medians of the SPEC values for fixed ω_τ (statistics $L_2(\omega_\tau)$); and
- $a_n = 4/N$ for $n \in [3N/4, N)$ and $a_n = 0$ elsewhere, i.e., for the highest magnitude SPEC samples (statistics $L_3(\omega_\tau)$).

It can be seen that for the median ($L_2(\omega_\tau)$), Figure 4c, the frequency region of stationary components is noticeable. However, from this illustration it is difficult to recognize that there are three components along the y-direction. From Figure 4b, again, the region of stationary components can be seen. In addition, from three peeks we can make the conclusion that scatterers are located at three different y-positions. In addition to the complex sinusoidal components in the third case, Figure 4d, the sinusoidal FM signal region can be seen. These three simple functions will be used in the construction of indicators for the region of rigid body and the region of rotating parts. Several modifications will also be made in order to take the advantage of the two-dimensional structure of the signal $q(\tau, m)$, as well as to keep the calculation burden within a reasonable limit.

3.3 Algorithm

Let us introduce the following notation: $I(\omega_\tau, \omega_m) = I_{\text{RIG}}(\omega_\tau, \omega_m) \cup I_{\text{MOV}}(\omega_\tau, \omega_m)$, where $I(\omega_\tau, \omega_m)$ is a function indicating the region in the range/cross-range domain with components caused by target (both from the rigid and rotating parts), while $I_{\text{RIG}}(\omega_\tau, \omega_m)$ is the region of rigid part; and $I_{\text{MOV}}(\omega_\tau, \omega_m)$ is the region of moving parts. In general, $I_{\text{RIG}}(\omega_\tau, \omega_m) \cap I_{\text{MOV}}(\omega_\tau, \omega_m) \neq \emptyset$ holds. The domain (ω_τ, ω_m) will be referred hereafter as the range/cross-range domain, since it can be easily transferred to the positions (x, y) of the radar target.

As an indicator of target in the range/cross-range domain the following simple criterion will be used:

$$I(\omega_\tau, \omega_m) = \begin{cases} 1 & |Q(\omega_\tau, \omega_m)| > \frac{1}{MN} \sum_{\omega_\tau} \sum_{\omega_m} |Q(\omega_\tau, \omega_m)| \\ 0 & \text{elsewhere,} \end{cases} \tag{19}$$

where $Q(\omega_\tau, \omega_m)$ is a 2D FT of $q(\tau, m)$. This is a very conservative measure, since the global threshold used here is equal to the mean of $|Q(\omega_\tau, \omega_m)|$, calculated in the entire range/cross-range domain.

Consider a 2D SPEC of the received signal:

$$SPEC(\tau, \omega_\tau; m, \omega_m; N_w, M_w) =$$

$$\left| \int_{-\infty}^{\infty} \sum_{\Delta m=0}^{M-1} q(\tau + \tau_w, m + \Delta m) w(\tau_w, \Delta m) e^{-j\omega_\tau \tau_w - j\omega_m \Delta m} d\tau_w \right|^2 . \tag{20}$$

The parameters N_w, M_w are added to denote the size of the window function $w(\tau_w, \Delta m)$ in the corresponding directions. The window width M_w is selected as $M_w \approx M$ (number of chirps). However, the narrow windows in the τ direction are used in order to control the concentration of the sinusoidal FM patterns caused by the rotating points. Namely, if the window is very wide the TF representation of the sinusoidal FM signal will look like several quasi stationary components [14], see Figure 3b. By decreasing the window width we are achieving a better concentration of these components around the instantaneous frequency of the sinusoidal FM components. Of course, if we decrease the window length too much, the frequency resolution will be decreased and semiperiods of this signal will be connected, resulting again in TF representation degradation.

The above analysis confirms that, in determination of the indicator function, the SPECs should be calculated with various window lengths. We will assume that

window lengths are selected from a set $N_w \in \mathbf{N}$, for constant M_w. The SPEC will not be evaluated for each (τ, m), but only for equidistantly spaced instants along the τ direction. The positions are separated for ΔT_{N_w} (for different windows different intervals are used; in our calculation study they are $\Delta T_{N_w} = T_c N/N_w$, $N_w \leq N$). Then, for each point in the range/cross-range domain we calculate:

$$L_{i,N_w}(\omega_\tau, \omega_m) = \sum_{i=0}^{N-1} a_n S_{(n)}(\omega_\tau, \omega_m), \; i = 1, 2, 3 \tag{21}$$

where $S_{(n)}(\omega_\tau, \omega_m)$ are elements from the set:

$$\mathbf{S}_{N_w} = \{SPEC(\tau, \omega_\tau; m, \omega_m; N_w, M_w), \; \tau = \tau' + l\Delta T_{N_w}, l \in Z\} \tag{22}$$

sorted into a non-decreasing order $S_{(n)}(\omega_\tau, \omega_m) \leq S_{(n+1)}(\omega_\tau, \omega_m)$. The index i denotes an earlier introduced form of L-statistics, while N_w denotes length of the window function. Based on the above considerations, we get the function for the rigid part (sinusoidal components):

$$I_{\text{RIG}}(\omega_\tau, \omega_m) = I(\omega_\tau, \omega_m) \prod_{N_w \subset \mathbf{N}} I'_{N_w}(\omega_\tau, \omega_m), \tag{23}$$

where $I'_{N_w}(\omega_\tau, \omega_m)$ can be defined as

$$I'_{N_w}(\omega_\tau, \omega_m) = \begin{cases} & L_{1,N_w}(\omega_\tau, \omega_m) \geq \frac{1}{MN} \sum_{\omega_\tau} \sum_{\omega_m} |L_{1,N_w}(\omega_\tau, \omega_m)| \text{ AND} \\ 1 & \frac{\sum_{k=-K_1}^{K_1} \sum_{l=-L_1}^{L_1} |L_{1,N_w}(\omega_\tau + k\Delta\omega_\tau, \omega_m + l\Delta\omega_m)|}{\sum_{k=-K_2}^{K_2} \sum_{l=-L_2}^{L_2} |L_{1,N_w}(\omega_\tau + k\Delta\omega_\tau, \omega_m + l\Delta\omega_m)|} \geq \frac{(2K_1+1)(2L_1+1)}{(2K_2+1)(2L_2+1)} \\ 0 & \text{otherwise.} \end{cases} \tag{24}$$

The first condition in (24) is equivalent to (19), while the second condition is introduced to further emphasize the local maxima, corresponding to the scattering points. It compares values of L_{1,N_w} samples (smallest SPEC samples) in a close neighborhood of the considered point (ω_τ, ω_m) with those in a wider neighborhood ($K_1 < K_2$ and $L_1 < L_2$).

For the widest window from the set, the function $|L_{1,N_w}(\omega_\tau + k_1\Delta\omega_\tau, \omega_m + l_1\Delta\omega_m)|$ would be well concentrated around the frequency of the rigid body signal components. The sinusoidal FM components, that are spread in the TF plane (see Figure 3a), could have high values of this function. However, for a narrow window, the function $|L_{1,N_w}(\omega_\tau + k_1\Delta\omega_\tau, \omega_m + l_1\Delta\omega_m)|$ would be spread around the rigid

body components, while the rotation components will be eliminated. Therefore, the product of $I'_{N_w}(\omega_\tau, \omega_m)$ in (23) will produce the function that is equal to 1 for a very narrow region in the range/cross-range domain (as in the case of wide window) with eliminated influence of the rotation parts (as in the case of using narrow window).

The remaining problem is determining the patterns representing the moving objects. The indication of moving object parts is described as:

$$I_{\text{MOV}}(\omega_\tau, \omega_m) = I(\omega_\tau, \omega_m) I''_{N_w}(\omega_\tau, \omega_m) \Lambda(\omega_\tau, \omega_m) \tag{25}$$

where:

$$I''_{N_w}(\omega_\tau, \omega_m) = \begin{cases} 1 & L_{3,N_w}(\omega_\tau, \omega_m) \geq (1+\beta) L_{2,N_w}(\omega_\tau, \omega_m) \\ 0 & \text{otherwise.} \end{cases} \tag{26}$$

The indicator function $I''_{N_w}(\omega_\tau, \omega_m)$ will be equal to 1 for regions in the range/cross-range domain where the ratio between the highest and the median SPEC samples is higher than $(1+\beta)$, where β is a threshold value. In our analysis $\beta = 1$ is used. This indicates that, along with the stationary pattern, there could exist a pattern caused by the moving objects, increasing the values of the SPEC at some instants of the TF plane. The remaining problem is to remove possible influence of the side lobes caused by the stationary pattern from the product $I(\omega_\tau, \omega_m) I''_{N_w}(\omega_\tau, \omega_m)$. To this aim we form a function $\Lambda(\omega_\tau, \omega_m)$ as:

$$\Lambda(\omega_\tau, \omega_m) = 1 - \text{dilate}(I_{\text{RIG}}(\omega_\tau, \omega_m)) \tag{27}$$

where "dilate" denotes the dilatation, a morphological operation that extends argument matrix (under extension we assume that the neighboring region around $I_{\text{RIG}}(\omega_\tau, \omega_m) = 1$ becomes also equal to 1) [15]. Function $\text{dilate}(I_{\text{RIG}}(\omega_\tau, \omega_m))$ for 3x3 closest samples in the range/cross-range domain can be defined as:

$$\text{dilate}(I_{\text{RIG}}(\omega_\tau, \omega_m)) = \bigvee_{k=-1}^{1} \bigvee_{l=-1}^{1} I_{\text{RIG}}(\omega_\tau + l\Delta\omega_\tau, \omega_m + k\Delta\omega_m), \tag{28}$$

where $\bigvee_{k=-1}^{1} a(k) = a(-1) \vee a(0) \vee a(1)$. This form is a dilatation with structural element square. We have introduced the dilatation since the indicator function $I_{\text{RIG}}(\omega_\tau, \omega_m)$ is very sharp. It also includes corresponding peaks only in the

Step 1.	Calculation of $SPEC(\tau, \omega_\tau; m, \omega_m; N_w, M_w)$, $\tau = \tau' + l\Delta T_{N_w}, l \in Z$ in equidistantly spaced points for windows N_w from set **N** that contains both wide and narrow windows. The interval ΔT_{N_w} is selected to be $\Delta T_{N_w} = T_r N/N_w$ where N is the widest window from the set.
Step 2.	Determination of the radar image as 2D DFT of signal $q(\tau, m)$, $Q(\omega_\tau, \omega_m)$.
Step 3.	Determination of region-of-nterest $I(\omega_\tau, \omega_m)$ by (19).
Step 4.	Calculation of order statistics $L_{i,N_w}(\omega_\tau, \omega_m)$, $i = 1, 2, 3$, (21), and for all the windows from set **N**.
Step 5.	Determination of the indicator functions $I'_{N_w}(\omega_\tau, \omega_m)$ by using (24).
Step 6.	Calculation of region-of-interest function for rigid body $I_{\text{RIG}}(\omega_\tau, \omega_m) = I(\omega_\tau, \omega_m) \prod_{N_w \subset \mathbf{N}} I'_{N_w}(\omega_\tau, \omega_m)$.
Step 7.	Calculation of $I''_{N_w}(\omega_\tau, \omega_m)$ by using (26).
Step 8.	Calculation of $\Lambda(\omega_\tau, \omega_m)$ by using (27).
Step 9.	Evaluation of the indicator function for the part of range/cross-range domain caused by moving parts $I_{\text{MOV}}(\omega_\tau, \omega_m) = I(\omega_\tau, \omega_m) I''_{N_w}(\omega_\tau, \omega_m) \Lambda(\omega_\tau, \omega_m)$.
Step 10.	Signal caused by rigid body and moving parts can be reconstructed as: $q_{\text{RIG}}(t, m) = IFT\{Q(\omega_\tau, \omega_m) I_{\text{RIG}}(\omega_\tau, \omega_m)\}$ and $q_{\text{MOV}}(t, m) = IFT\{Q(\omega_\tau, \omega_m) I_{\text{MOV}}(\omega_\tau, \omega_m)\}$.

Table 1: *Procedure for the radar image analysis.*

range/cross-range-domain. Therefore, the function $\Lambda(\omega_\tau, \omega_m)$ allows that points that are not close to the rigid body part could be identified as rotating parts.

For the separation of the rotating object component we can use the product $I_{\text{MOV}}(\omega_\tau, \omega_m) Q(\omega_\tau, \omega_m)$. Also, as it can be seen, in the case of moving parts detection, we did not employ the multiwindow approach, but only a single, relatively narrow, window. Namely, in this case, results obtained for extremely narrow and wide windows are not useful in the separation process, while for other windows results are very similar.

Note that the algorithm is derived based on the assumption that the rigid body influenced signal can be modeled as a sum of complex sinusoids. For more complicated target motion patterns, the motion compensation techniques for focusing the distorted data should be applied in the first stage of the algorithm [16].

The procedure for separation is summarized in Table 1.

4 The Radon transform based algorithm for the separation of sinusoidal FM signals

The second approach that will be presented in this section is based on the RT. It can be used only for the rotating parts of the target that produce pure sinusoidal FM signals. This approach can be applied only in the case when the influence of the rotating parts is emphatic.

The RT of a point with position (x_r, y_r) is

$$R_r(\rho, \theta) = c_r \delta(\rho - A_r \sin(\theta - \varphi_r)), \tag{29}$$

where c_r corresponds to the reflection of the point, $A = \sqrt{x_r^2 + y_r^2}$ and $\varphi_r = \tan^{-1}(y_r/x_r)$. The period of the RT in θ is 2π. It means that the inverse RT of a sinusoidal pattern in the (θ, ρ) plane is a point in the (x_r, y_r) domain. Since the rotating parts produce sinusoidal patterns in the TF domain, it means that the inverse RT of the TF representation of the received signal with m-D effects will have peaks at the positions corresponding to the rotating parts. Note that for the inverse RT we should know the period of the sinusoidal pattern, which is not known in advance. In addition, the radar signal may consist of several rotating parts with different unknown rotation frequencies. To solve this problem we assigned the considered time interval (in the TF representation) to a set of possible periods in θ. The whole TF representation is considered as periodic in time with T_p corresponding to periods in θ, for example from $\pi/3$ up to 4π with a step of 0.1π. The value of 4π means that exactly two periods of sinusoidal pattern exist in the TF representation.

When the assumed period matches the true one, the peak in the inverse RT is detected at a position defined by $A = \sqrt{x_r^2 + y_r^2}$ and $\varphi_r = \tan^{-1}(y_r/x_r)$. In this way, all the parameters of the rotating part are known, including the frequency of the rotation that corresponds to the period assigned for the case where the peak is found. If there are more than one rotating part, with different or the same rotation speed, more peaks will be detected. By filtering the region around the peak and calculating the RT of the filtered inverse RT, we get a clear TF representation of the signal resulting from the rotating parts.

5 Results

5.1 Example 1:

In the first example we considered the simulation setup described in Section 3 and used in [8]. The radar image, including the notable m-D effect, is depicted in Figure 5a. The algorithm described in Section 3 is applied. The Hanning windows are employed along both directions with $M_w = M$ and the set of window lengths in $\mathbf{N} = \{512, 256, 128, 64, 32, 16, 8\}$ is used. In the calculation of $I_{\text{RIG}}(\omega_\tau, \omega_m)$, the expression (23) is applied, where the product $\prod_{N_w \subset \mathbf{N}} I'_{N_w}(\omega_\tau, \omega_m)$ is calculated iteratively starting from the widest toward narrower windows from the set N. If the resulting product is not changed in consecutive iterations we can stop the procedure. This is an important step, since it significantly reduces the calculations in the case of targets without m-D effect. The obtained radar image of the rigid body is depicted in Figure 5b. The parameters $K_1 = L_1 = 1$ and $K_2 = L_2 = 3$ are used in (24). It can be seen that excellent accuracy is achieved. We calculated the region of sinusoidal FM component by using (25), with $N_w = 64$. The region of sinusoidal FM signals is given in Figure 5c. In order to demonstrate the accuracy of this approach, the reconstruction of the sinusoidal FM signal for $m = 0$ is given in Figure 5d. The sinusoidal FM component can easily be recognized from this illustration. At the same time some important features of the moving object can be extracted.

5.1.1 Vibration

This setup has been used for the alternative experiment. The same target, but without rotating parts, has been considered. However, the entire target oscillates in the x direction with amplitude of 0.1 cm and frequency of oscillations 30 Hz. The obtained results are presented in Figure 6. A significant improvement in radar imagining is achieved with the proposed technique. At the same time, this technique can be used for extraction of the vibration parameters. Note that an analysis of m-D effect for vibrating targets in SAR systems is given in [9], [17].

5.2 Example 2

A more complex object, with 45 scatterers: $\{(k, 0)$ for $k \in [-6, 6]$, $(0, k)$ for $k \in [-6, -1] \cup [1, 6]$, $(k, \pm(6 - k))$ for $k \in [1, 5]$ and $(k, \pm(6 + k))$ for $k \in [-5, -1]\}$, is considered. All scatterers have the same reflection coefficient, set to 2. There are two rotating parts. The first rotating part is the same as in the previous example, while the second rotating part rotates at a rate of 2 Hz and a rotation radius of 0.5 m from center. The reflection of the second rotating part has been set to 7. The same analysis, with the same algorithm setup, like in the previous example is performed. Obtained results are depicted in Figure 7. It can be seen that the reconstruction of

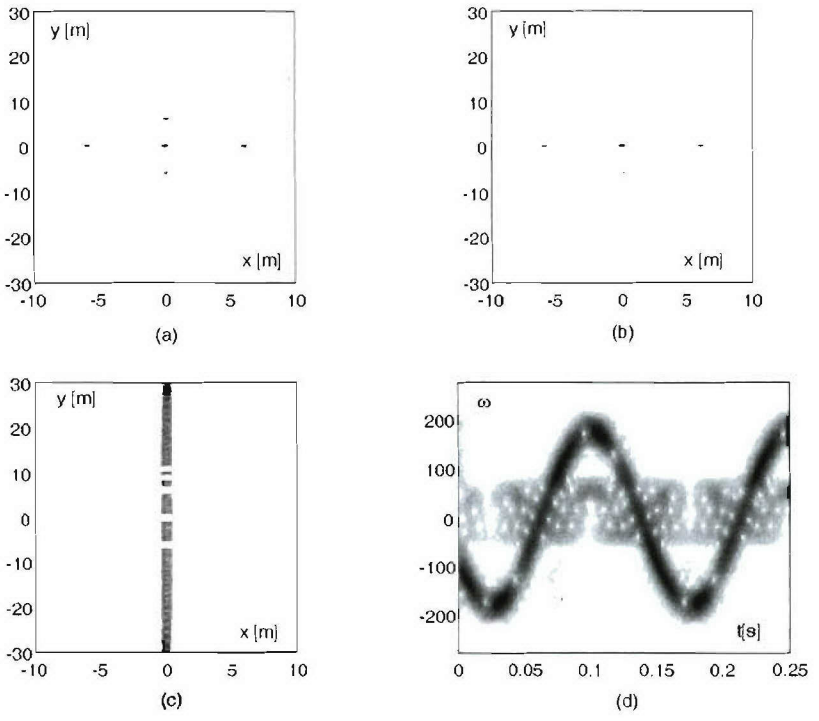

Figure 5: *Separation of rigid body and m-D effect for simple case: (a) $Q(\omega_\tau, \omega_m)$; (b) Reconstructed radar image; (c) Region of support for the sinusoidal FM signal; (d) SPEC of the reconstructed m-D signal.*

objects has been done in a very accurate way. At the same time, the reconstruction of the signal caused by the rotating parts is good.

5.3 Radon transform based algorithm

In this case we also apply the inverse RT, assuming that the TF representation pattern is periodic with periods from $\pi/3$ to 3π, with step of $\pi/18$. Two peaks of the inverse RT concentration are detected at two different periods, amplitudes and phases, see Figure 8. Calculating the RT of the inverse RT filtered around these peaks, we obtained the representation presented in Figure 9, producing very accurate reconstruction of the rotating parts in the TF domain.

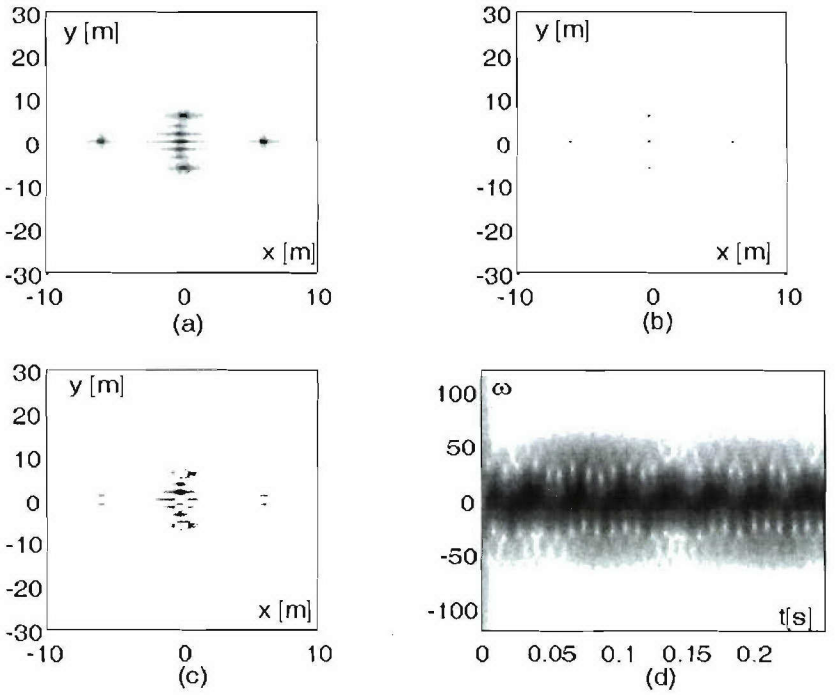

Figure 6: *Separation of rigid body and m-D effect caused by object vibrations: (a) $Q(\omega_\tau, \omega_m)$; (b) Reconstructed radar image; (c) Region of support for the signal caused by vibrations; (d) Spectrogram of the reconstructed m-D signal.*

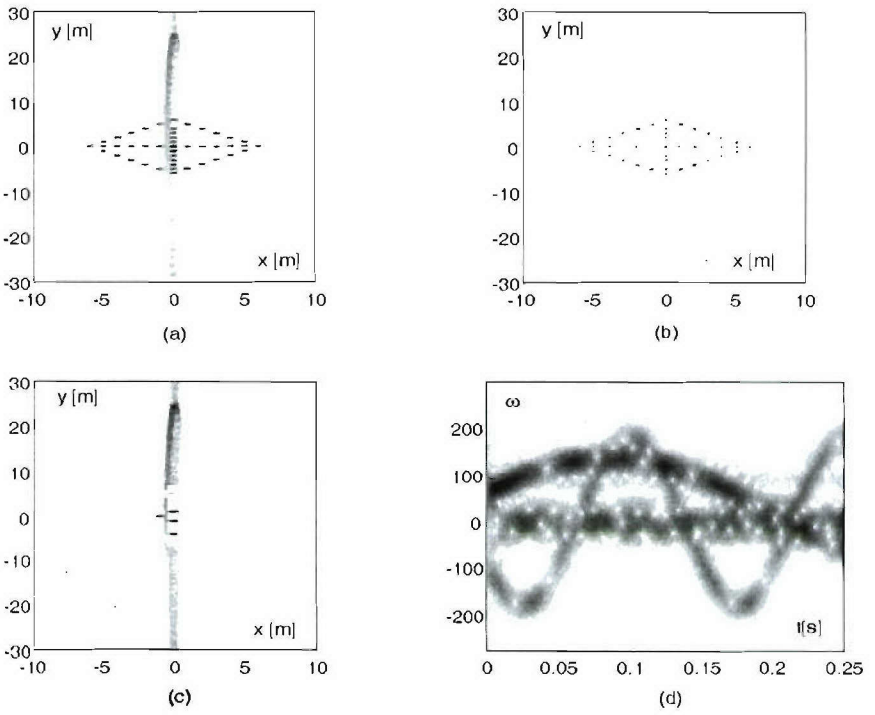

Figure 7: *Separation of rigid body and m-D effect for two moving points: (a)* $Q(\omega_\tau, \omega_m)$*; (b) Reconstructed radar image; (c) Region of support for the sinusoidal FM signal; (d) SPEC of the reconstructed m-D signal.*

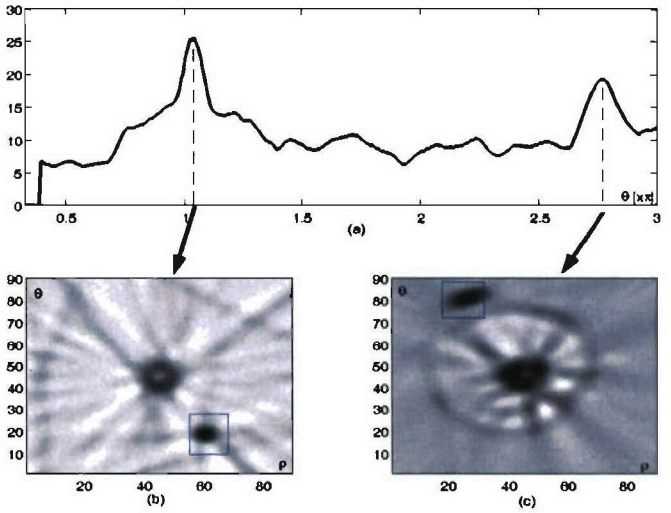

Figure 8: *Concentration measure of the inverse RT of the radar signal TF representation as a function of the assumed angle number (top), with the inverse RT at two positions where maxima are found (bottom).*

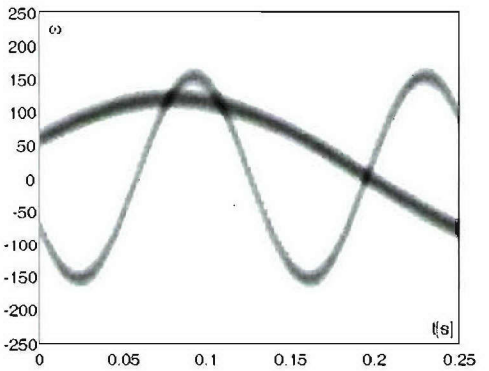

Figure 9: *TF representation corresponding to the rotating parts in the last example, obtained by using filtered inverse RT. The x-axis corresponds to range time and the y-axis corresponds to frequency.*

5.4 UH-1D Helicopter

In this example we consider the simulated signal of a German Air Force Bell UH-1D Helicopter known also as 'Iroquois'. The simulation is performed according to [4]. Several effects are emphasized in the TF representation Figure 10. The stationary patterns along the time-axis correspond to the rigid body reflection, the vibration of the target or the radar-clutter caused by the moving in the target background. The motion of the two main blades is modeled by two rotating reflectors, producing sinusoidal FM signals with a large magnitude in the frequency direction, (15). The main rotor flashes are simulated by the signals producing lines connecting peaks of the sinusoidal FM signal with time axis. The smaller pulses that can be seen in the right hand side of Figure 10a correspond to the tail rotor flashes. These flashes correspond to periodic alignment of the main and tail rotors to maximally reflect the radar signal. Note that other effects that can be observed in a radar image, including multipath, are not considered here.

Therefore, the simplified model of the reflected UH-1D signal can be written as:

$$x(t) = x_{RIG}(t) + x_{ROT}(t) + x_{FL\_M}(t) + x_{FL\_T}(t),$$

where $x_{RIG}(t)$, $x_{ROT}(t)$, $x_{FL\_M}(t)$ and $x_{FL\_T}(t)$ represent signals caused by the rigid body, rotation of the main rotor, and the main and tail rotor flashes, respectively. The signal is considered within the interval of 400 ms, sampled with a rate of $\Delta t = 1/48000$ s. Four sinusoidal components, caused by the rigid body, are at the frequencies -10.3 kHz, -2.5 kHz, 2.3 kHz and 2.7 kHz. Two components at -0.4 kHz and 0.4 kHz correspond to the modulated time tones commonly added to the data tape [18]. The sinusoidal FM signals, corresponding to the rotation of the main rotor blades, are modeled as:

$$x_{ROT}(t) = \sigma_{ROT}[\exp(j2\pi A_{ROT}\sin(2\pi t/T_{ROT})) + \exp(-j2\pi A_{ROT}\sin(2\pi t/T_{ROT}))]. \tag{30}$$

where $T_{ROT} = 175$ ms and $A_{ROT} = 19$ kHz. The main and tail rotor flashes are modeled as broadband pulses given as:

$$\begin{aligned} x_{FL\_M}(t) &= \sigma_{FL\_M}\sum_k \delta(t - kT_{ROT}/2) *_\tau h_{FL\_M}(t) \\ x_{FL\_T}(t) &= \sigma_{FL\_T}\sum_k \delta(t - kT_{TAIL}/2) *_\tau h_{FL\_T}(t), \end{aligned} \tag{31}$$

where T_{TAIL} in our experiment is $T_{TAIL} = 35.8\,\text{ms}$, while $h_{FL\_M}(t)$ and $h_{FL\_T}(t)$ are cut-off filters given in the frequency domain as:

$$H_{FL\_M}(\omega) = \begin{cases} 1 & |\omega| < 2\pi A_{ROT} \\ 0 & \text{elsewhere,} \end{cases}$$

$$H_{FL\_T}(\omega) = \begin{cases} 1 & 2\pi(7.35\,\text{kHz}) < \omega < 2\pi(15.7\,\text{kHz}) \\ 0 & \text{elsewhere.} \end{cases}$$

The signal is corrupted with the moderate Gaussian noise. To compare our simulated radar image with the real one, refer to [4, 18].

The previously used form of the L-statistics can be applied for separation of the rigid body and rotating parts influence. In the case when we want to separate the different effects caused by the rotating parts, the modified L-statistics can be applied. The L-statistics corresponding to the smallest SPEC samples is presented in Figure 10b. As a threshold we adopted 10% of the maximal value of the corresponding L-statistics. The dotted line represents the region of detected stationary patterns. For the detection of the tail blades region we have considered L-statistics of 30% the highest SPEC samples for each frequency, excluding 10% the highest ones of them (Figure 10c). Again, the region is estimated based on the values that are above 10% of the maximal value of the L-statistics, but with excluded stationary components regions. Finally, the highest 10% of SPEC samples are given in Figure 10d. Based on this illustration, it is easy to determine the region of the main blades (comparing to the threshold determined as in previous cases, but not excluding any sample). The separation of the target components is shown in Figure 11.

Note that the proposed approach can be used for helicopter radar signals where relatively long FM signal components appear. In the case when, in the recording, short burst components dominate, on high frequencies, without a sinusoidal FM component, wavelet transform analysis setup can be efficiently used [1].

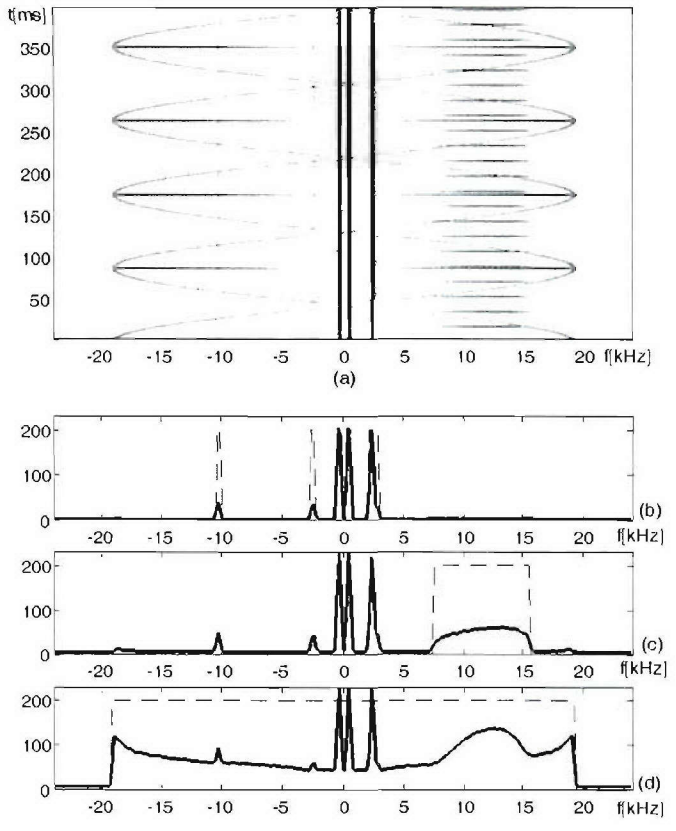

Figure 10: *Radar imaging of the simulated helicopter signal: (a) TF representation; (b) Detection of the stationary patterns; (c) Detection of the tail-blades; (d) Detection of the main blades region.*

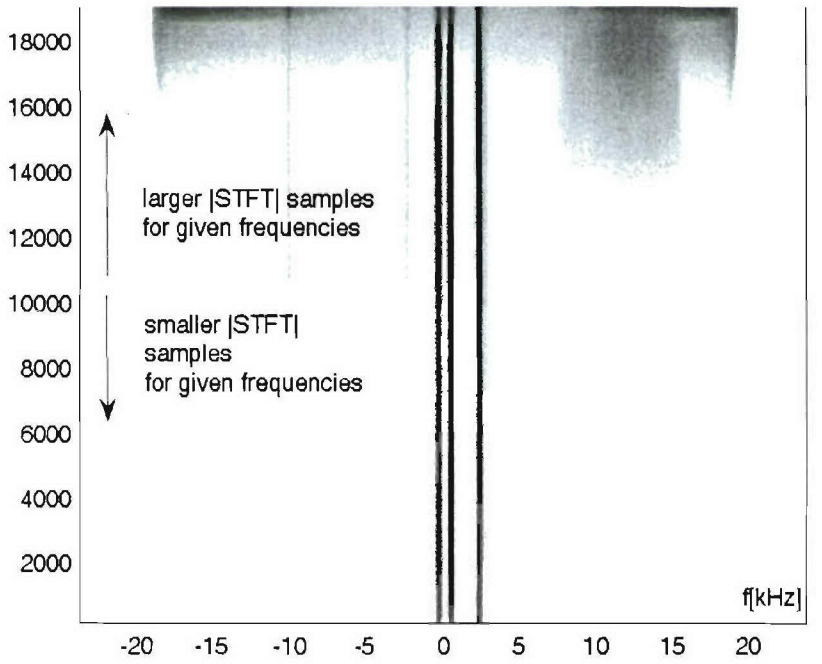

Figure 11: *Sorted spectrogram samples to obtain L-statistics*

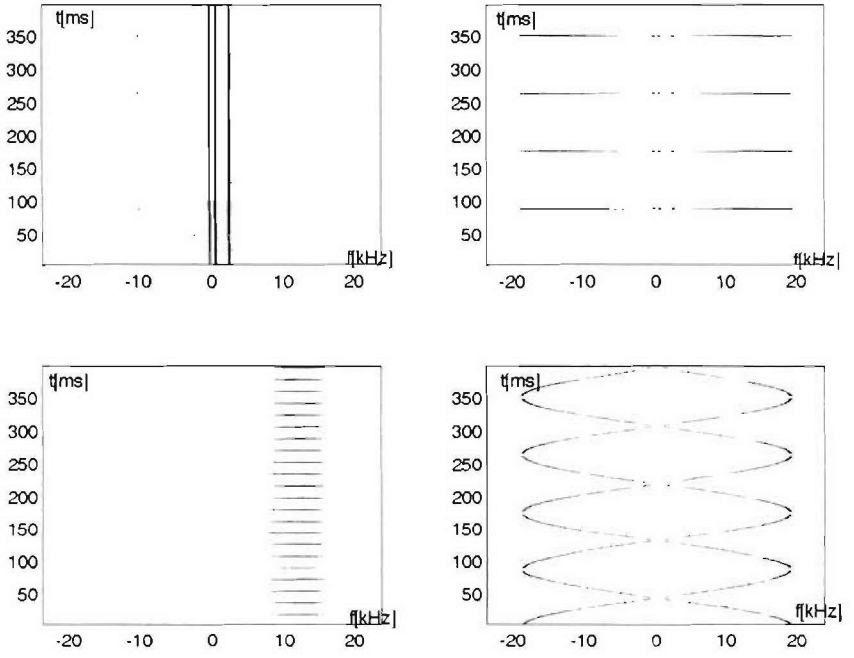

Figure 12: *Separation of components of the target: stationary signal pattern (top, left); main rotor flashes (top, right); tail rotor flashes (bottom, left); rotating blades (bottom, right).*

6 CONCLUSION

Two techniques for separating the rigid body radar image from micro-Doppler effect caused signal in ISAR/SAR imaging are proposed. The first technique is based on the order statistics of the SPEC samples. In order to separate the patterns caused by the rotating and rigid body parts, a spectrogram is evaluated for various window sizes. The spectrogram evaluated with a narrow window produces a high concentration of the signal caused by rotating parts, while a spectrogram evaluated for a wide window produces a high concentration of the signal corresponding to the rigid body parts. The second approach is based on the Radon transform processing of obtained radar signals. It can be useful in the case of the radar targets with a dominant micro-Doppler effect caused signals. Both proposed methods have shown satisfactory accuracy for the considered complex simulated examples, including rotating and vibrating target parts.

This report provides the preliminary ground work for this challenging field of research. There is room for improvement of the algorithm in terms of accuracy and adaptability. Two components of the algorithm, i.e., spectrogram and sorting of samples, can be further studied in order to improve the performance of the algorithm. For example, fast sorting procedures such as quicksort or insertion sort can be investigated and employed to reduce the calculation burden of the procedure.

This report also demonstrates that whenever the target has one or more rotating or vibrating parts, the frequency modulations on the returned signal can introduce large distortion in the SAR/ISAR images. On the other hand, the m-D effect also carries information about the features of moving parts of the target that are complementary to those existing recognition methods. The proposed method not only can focus the distorted SAR/ISAR images, but also can provide additional information about the rotating/vibrating features of the target. Therefore, new algorithms and methods will have to be further investigated to separate the stationary and non-stationary components of the target of interest.

Annex A
L-statistic

This section provides a step by step procedure of the L-statistics method described in Section 3 to separate the rigid and rotating parts of the target. The procedure is given here in numerical example to visualize the methodology. Assume that we have a signal with three sinusoidal components and a sinusoidal FM signal. Here, we will consider the synthetic time-frequency plane with just 21x21 samples. We will also assume that the spectrograms calculated in the tables are with wide, middle and narrow size windows. The goal is to separate the sinusoidal components (caused by the rigid body) and sinusoidal FM signal (caused by a rotating part).

Consider a simplified matrix of the signal values in the time-frequency given in the next table. As it will be shown later the same situation appears in practical real examples.

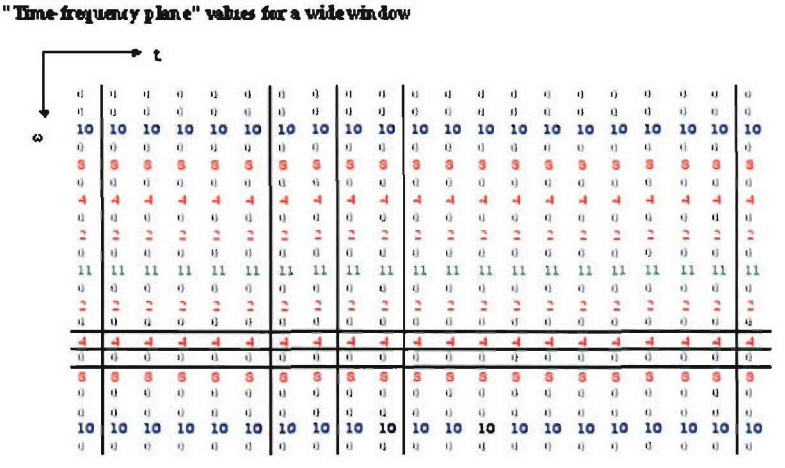

The blue color represents sinusoidal component caused by rigid body. The red color is for the part caused by sinusoidal FM signal, here distorted (due to the wide window) to quasi-sinusoids. The green color are the samples influenced by both sinusoidal FM signals and sinusoids. Assume that for each frequency we perform the sorting in time from the smallest toward the highest values. In this case, since the values in time do not change, we obtained in fact the same time-frequency representation.

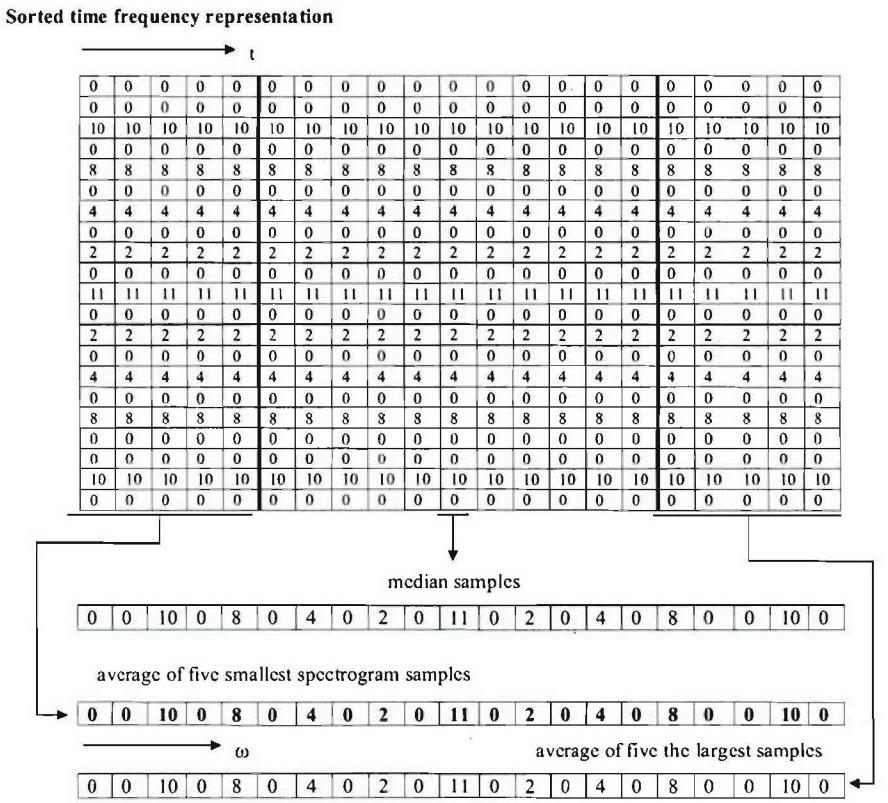

The smallest samples are used to indicate the region of the sinusoidal components (caused by the rigid body). Assume that the indication function for the wide window is calculated as a region with the smallest signal samples different from 0. We obtain:

However, the results obtained with the wide window are not a good indication for a region of rigid body part since they include the influence of the sinusoidal FM signal.

"Time-frequency plane" for a narrow window

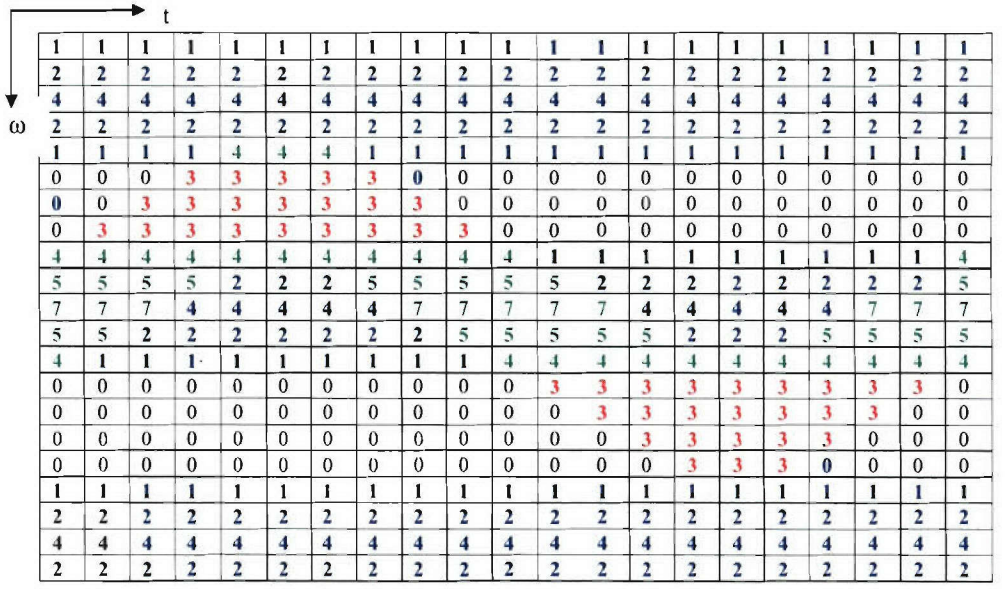

1	1	1	1	1	1	1	1	1	1	1	1	1	1	1	1	1	1	1	1	1	1
2	2	2	2	2	2	2	2	2	2	2	2	2	2	2	2	2	2	2	2	2	2
4	4	4	4	4	4	4	4	4	4	4	4	4	4	4	4	4	4	4	4	4	4
2	2	2	2	2	2	2	2	2	2	2	2	2	2	2	2	2	2	2	2	2	2
1	1	1	1	4	4	4	1	1	1	1	1	1	1	1	1	1	1	1	1	1	1
0	0	0	3	3	3	3	3	0	0	0	0	0	0	0	0	0	0	0	0	0	0
0	0	3	3	3	3	3	3	3	0	0	0	0	0	0	0	0	0	0	0	0	0
0	3	3	3	3	3	3	3	3	3	0	0	0	0	0	0	0	0	0	0	0	0
4	4	4	4	4	4	4	4	4	4	4	1	1	1	1	1	1	1	1	1	1	4
5	5	5	5	2	2	2	5	5	5	5	5	2	2	2	2	2	2	2	2	2	5
7	7	7	4	4	4	4	4	7	7	7	7	7	4	4	4	4	4	7	7	7	
5	5	2	2	2	2	2	2	2	5	5	5	5	5	2	2	2	5	5	5	5	
4	1	1	1	1	1	1	1	1	1	4	4	4	4	4	4	4	4	4	4	4	
0	0	0	0	0	0	0	0	0	0	0	3	3	3	3	3	3	3	3	3	0	
0	0	0	0	0	0	0	0	0	0	0	0	3	3	3	3	3	3	3	0	0	
0	0	0	0	0	0	0	0	0	0	0	0	0	3	3	3	3	3	0	0	0	
0	0	0	0	0	0	0	0	0	0	0	0	0	0	3	3	3	0	0	0	0	
1	1	1	1	1	1	1	1	1	1	1	1	1	1	1	1	1	1	1	1	1	
2	2	2	2	2	2	2	2	2	2	2	2	2	2	2	2	2	2	2	2	2	
4	4	4	4	4	4	4	4	4	4	4	4	4	4	4	4	4	4	4	4	4	
2	2	2	2	2	2	2	2	2	2	2	2	2	2	2	2	2	2	2	2	2	

"Sorted TF plane"

1	1	1	1	1	1	1	1	1	1	1	1	1	1	1	1	1	1	1	1	1
2	2	2	2	2	2	2	2	2	2	2	2	2	2	2	2	2	2	2	2	2
4	4	4	4	4	4	4	4	4	4	4	4	4	4	4	4	4	4	4	4	4
2	2	2	2	2	2	2	2	2	2	2	2	2	2	2	2	2	2	2	2	2
1	1	1	1	1	1	1	1	1	1	1	1	1	1	1	1	1	1	4	4	4
0	0	0	0	0	0	0	0	0	0	0	0	0	0	0	0	3	3	3	3	3
0	0	0	0	0	0	0	0	0	0	0	0	0	0	3	3	3	3	3	3	3
0	0	0	0	0	0	0	0	0	0	0	0	3	3	3	3	3	3	3	3	3
1	1	1	1	1	1	1	1	4	4	4	4	4	4	4	4	4	4	4	4	4
2	2	2	2	2	2	2	2	2	2	5	5	5	5	5	5	5	5	5	5	5
4	4	4	4	4	4	4	4	4	7	7	7	7	7	7	7	7	7	7	7	7
2	2	2	2	2	2	2	2	2	5	5	5	5	5	5	5	5	5	5	5	5
1	1	1	1	1	1	1	1	4	4	4	4	4	4	4	4	4	4	4	4	4
0	0	0	0	0	0	0	0	0	0	3	3	3	3	3	3	3	3	3	3	3
0	0	0	0	0	0	0	0	0	0	0	0	3	3	3	3	3	3	3	3	3
0	0	0	0	0	0	0	0	0	0	0	0	0	0	3	3	3	3	3	3	3
0	0	0	0	0	0	0	0	0	0	0	0	0	0	0	0	0	0	3	3	3
1	1	1	1	1	1	1	1	1	1	1	1	1	1	1	1	1	1	1	1	1
2	2	2	2	2	2	2	2	2	2	2	2	2	2	2	2	2	2	2	2	2
4	4	4	4	4	4	4	4	4	4	4	4	4	4	4	4	4	4	4	4	4
2	2	2	2	2	2	2	2	2	2	2	2	2	2	2	2	2	2	2	2	2

Average for the largest five samples

1	2	4	2	2.8	3	3	3	4	5	7	5	4	3	3	3	1.8	1	2	4	2

Median of samples

1	2	4	2	1	0	0	0	4	2	7	5	4	0	0	0	0	1	2	4	2

Average for the smallest five samples

1	2	4	2	1	0	0	0	1	2	4	2	1	0	0	0	0	1	2	4	2

$L_{1\,narrow\ window}(\omega)$

1	1	1	1	1	0	0	0	1	1	1	1	1	0	0	0	0	1	1	1	1

Spectrogram with a middle-sized window

ω \ t																					
	0	0	0	0	0	0	0	0	0	0	0	0	0	0	0	0	0	0	0	0	0
	2	2	2	2	2	2	2	2	2	2	2	2	2	2	2	2	2	2	2	2	2
	6	6	6	6	6	6	6	6	6	6	6	6	6	6	6	6	6	6	6	6	6
	2	2	2	2	2	2	2	2	2	2	2	2	2	2	2	2	2	2	2	2	2
	0	0	0	0	0	0	0	0	0	0	0	0	0	0	0	0	0	0	0	0	0
	0	0	0	0	5	5	5	0	0	0	0	0	0	0	0	0	0	0	0	0	0
	0	0	0	5	5	5	5	5	0	0	0	0	0	0	0	0	0	0	0	0	0
	0	0	5	5	5	5	5	5	5	0	0	0	0	0	0	0	0	0	0	0	0
	0	5	5	5	0	0	0	5	5	5	0	0	0	0	0	0	0	0	0	0	0
	7	7	7	2	2	2	2	2	7	7	7	2	2	2	2	2	2	2	2	2	7
	11	11	6	6	6	6	6	6	7	11	11	6	6	6	6	6	6	6	6	11	11
	7	2	2	2	2	2	2	2	2	2	7	7	7	2	2	2	2	2	7	7	7
	0	0	0	0	0	0	0	0	0	0	0	5	5	5	0	0	0	5	5	5	0
	0	0	0	0	0	0	0	0	0	0	0	0	5	5	5	5	5	5	5	0	0
	0	0	0	0	0	0	0	0	0	0	0	0	0	5	5	5	5	5	0	0	0
	0	0	0	0	0	0	0	0	0	0	0	0	0	0	5	5	5	0	0	0	0
	0	0	0	0	0	0	0	0	0	0	0	0	0	0	0	0	0	0	0	0	0
	0	0	0	0	0	0	0	0	0	0	0	0	0	0	0	0	0	0	0	0	0
	2	2	2	2	2	2	2	2	2	2	2	2	2	2	2	2	2	2	2	2	2
	6	6	6	6	6	6	6	6	6	6	6	6	6	6	6	6	6	6	6	6	6
	2	2	2	2	2	2	2	2	2	2	2	2	2	2	2	2	2	2	2	2	2

"Sorted TF plane"

0	0	0	0	0	0	0	0	0	0	0	0	0	0	0	0	0	0	0	0
2	2	2	2	2	2	2	2	2	2	2	2	2	2	2	2	2	2	2	2
6	6	6	6	6	6	6	6	6	6	6	6	6	6	6	6	6	6	6	6
2	2	2	2	2	2	2	2	2	2	2	2	2	2	2	2	2	2	2	2
0	0	0	0	0	0	0	0	0	0	0	0	0	0	0	0	0	0	0	0
0	0	0	0	0	0	0	0	0	0	0	0	0	0	0	0	0	5	5	5
0	0	0	0	0	0	0	0	0	0	0	0	0	0	0	5	5	5	5	5
0	0	0	0	0	0	0	0	0	0	0	0	0	5	5	5	5	5	5	5
0	0	0	0	0	0	0	0	0	0	0	0	0	0	5	5	5	5	5	5
2	2	2	2	2	2	2	2	2	2	2	2	2	7	7	7	7	7	7	7
6	6	6	6	6	6	6	6	6	6	6	6	6	6	11	11	11	11	11	11
2	2	2	2	2	2	2	2	2	2	2	2	2	7	7	7	7	7	7	7
0	0	0	0	0	0	0	0	0	0	0	0	0	0	5	5	5	5	5	5
0	0	0	0	0	0	0	0	0	0	0	0	0	5	5	5	5	5	5	5
0	0	0	0	0	0	0	0	0	0	0	0	0	0	0	5	5	5	5	5
0	0	0	0	0	0	0	0	0	0	0	0	0	0	0	0	0	5	5	5
0	0	0	0	0	0	0	0	0	0	0	0	0	0	0	0	0	0	0	0
0	0	0	0	0	0	0	0	0	0	0	0	0	0	0	0	0	0	0	0
2	2	2	2	2	2	2	2	2	2	2	2	2	2	2	2	2	2	2	2
6	6	6	6	6	6	6	6	6	6	6	6	6	6	6	6	6	6	6	6
2	2	2	2	2	2	2	2	2	2	2	2	2	2	2	2	2	2	2	2

Average of the largest five samples

0	2	6	2	0	3	5	5	5	7	11	7	5	5	5	3	0	0	2	6	2

Median of samples

0	2	6	2	0	0	0	0	0	2	6	2	0	0	0	0	0	0	2	6	2

Average of the smallest five samples

0	2	6	2	0	0	0	0	0	2	6	2	0	0	0	0	0	0	2	6	2

$L_{1\,\text{middle window}}(\omega)$

0	1	1	1	0	0	0	0	0	1	1	1	0	0	0	0	0	0	1	1	1

Now we can recall three functions L1 obtained for three various windows.

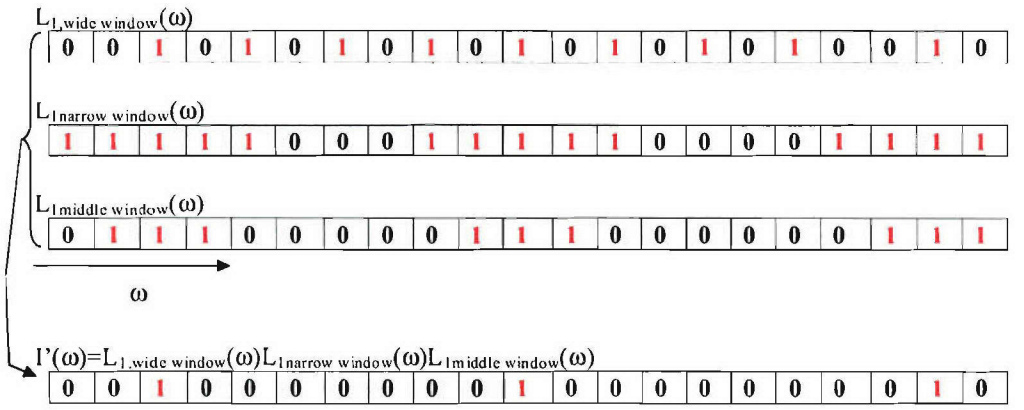

To obtain the detection function for the signal region caused by the rotating part it is enough to reconsider the time-frequency representation with middle window size, i.e., to consider the statistics of the highest and median samples for the middle window.

$L_3(\omega)$ Statistics for the largest samples

0	2	6	2	0	3	5	5	5	7	11	7	5	5	5	3	0	0	2	6	2

$L_2(\omega)$ Median of samples

0	2	6	2	0	0	0	0	0	2	6	2	0	0	0	0	0	0	2	6	2

$L_3(\omega)/L_2(\omega)$

0/0	1	1	1	0/0	inf	inf	inf	inf	3.5	1.83	3.5	inf	inf	inf	inf	0/0	0/0	1	1	1

$I''(w)=L_3(\omega)/L_2(\omega)>=(1+\beta)$, $\beta=1$ (0/0 treated as 0)

0	0	0	0	0	1	1	1	1	1	0	1	1	1	1	1	0	0	0	0	0

The pattern caused by the rotating part can be assumed to be the region of the TF plane distinct from 0 with $I''(\omega) = 1$

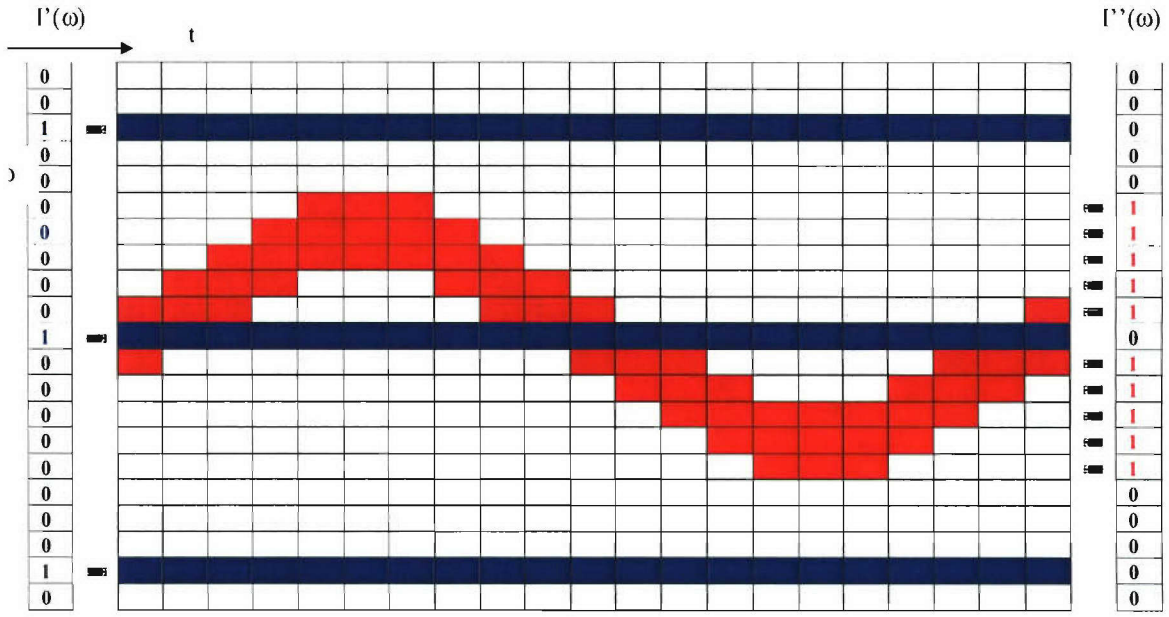

blue color rigid body influenced signal
red color rotating body influence

The following Figures A1-A13 illustrate the step by step procedure to separate the rigid and rotating parts of the body using the method described in Section 3. A similar signal, as in Section 3, is used in this example. Figure A1 shows the time-frequency representation of the signal with a very wide window and Figure A2 shows the sorted time-frequency representation. The statistics for the wide window case is shown in Figure A3. Figure A4 shows the time-frequency representation of the signal with middle window and Figure A5 shows the sorted time-frequency representation. The statistics for the middle window case is shown in Figure A6. Figure A7 shows the time-frequency representation of the signal with narrow window and Figure A8 shows the sorted time-frequency representation. The statistics for the narrow window case is shown in Figure A9. The indicator function for the stationary patterns (rigid body influence) is shown in Figure 10. Figure 11 shows the indicator function for sinusoidal FM signal patterns (rotating part influence). The reconstructed rigid body and rotating parts are shown in Figure 12 and Figure 13, respectively.

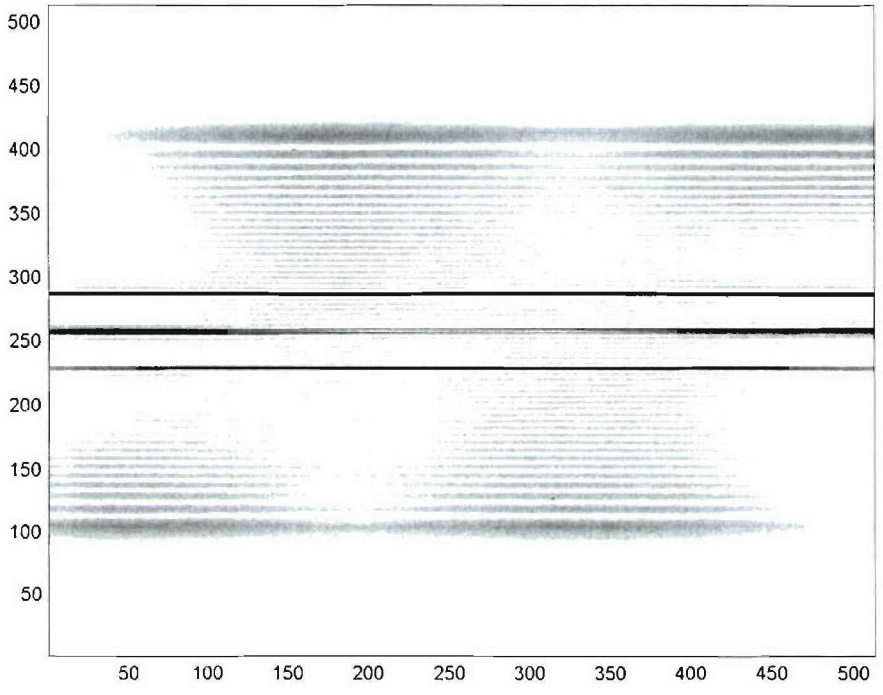

Figure A.1: *Time-frequency representation with very wide window*

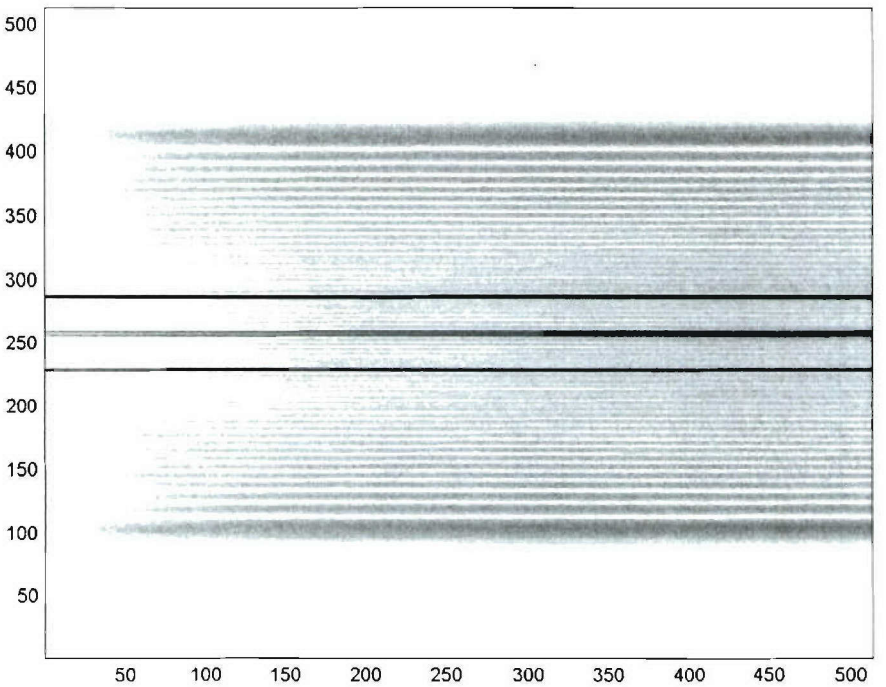

Figure A.2: *"Sorted" time-frequency representation*

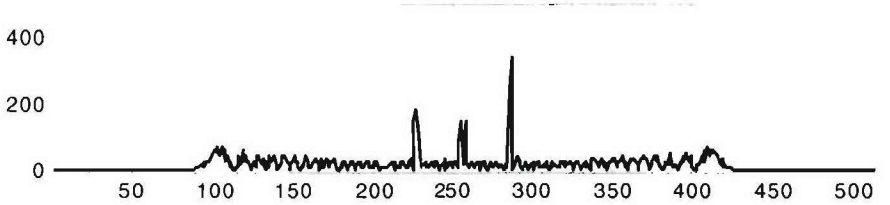

Figure A.3: *Statistics for the wide window case (L1 smallest samples, L2 median samples, and L3 highest samples)*

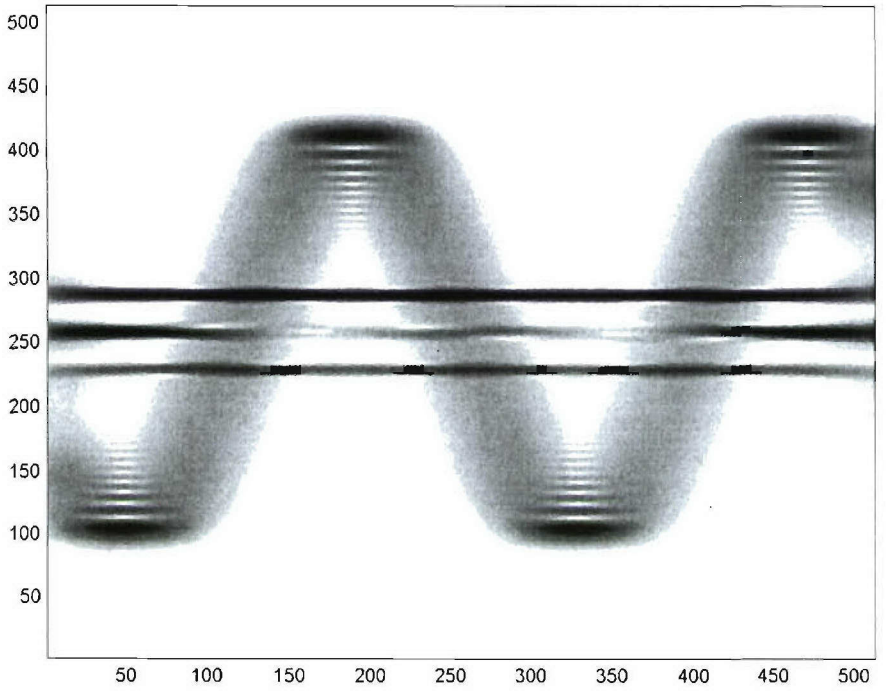

Figure A.4: *Time-frequency representation with middle window*

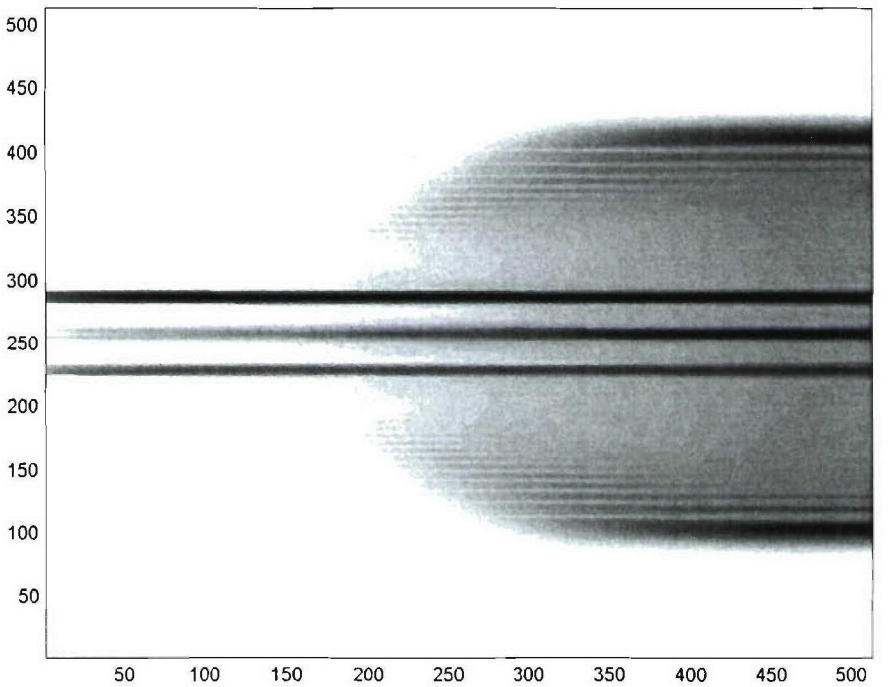

Figure A.5: *"Sorted" time-frequency representation*

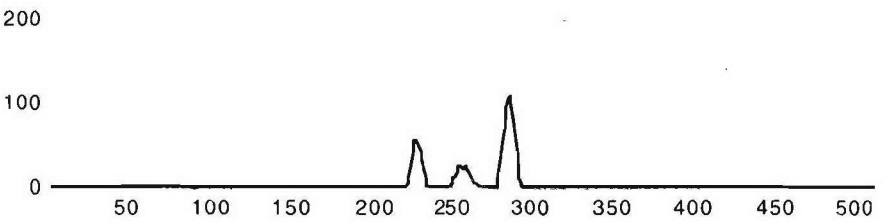

Figure A.6: *Statistics for the middle window case (L1 smallest samples, L2 median samples, and L3 highest samples)*

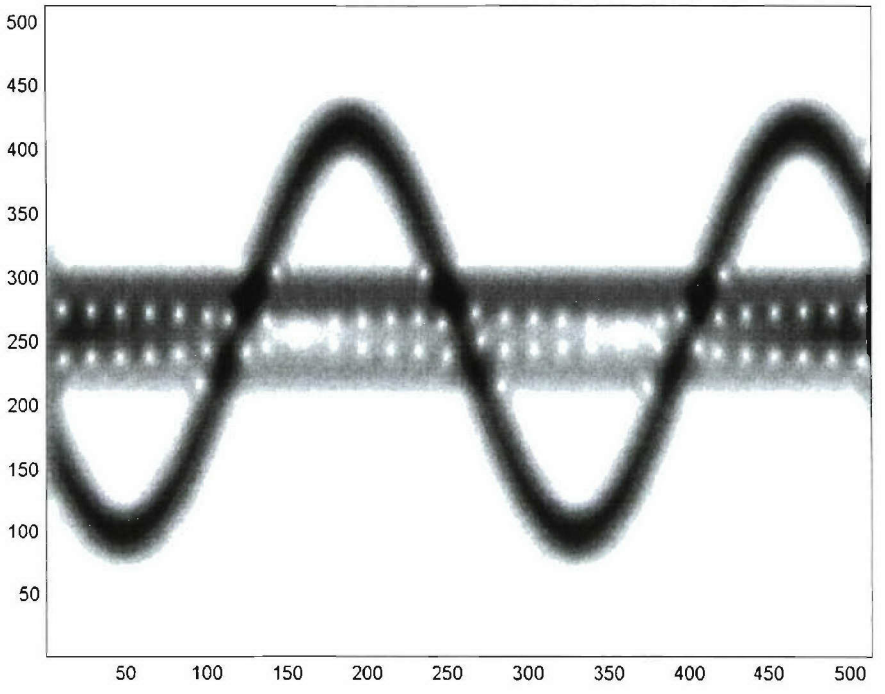

Figure A.7: *Time-frequency representation with narrow window*

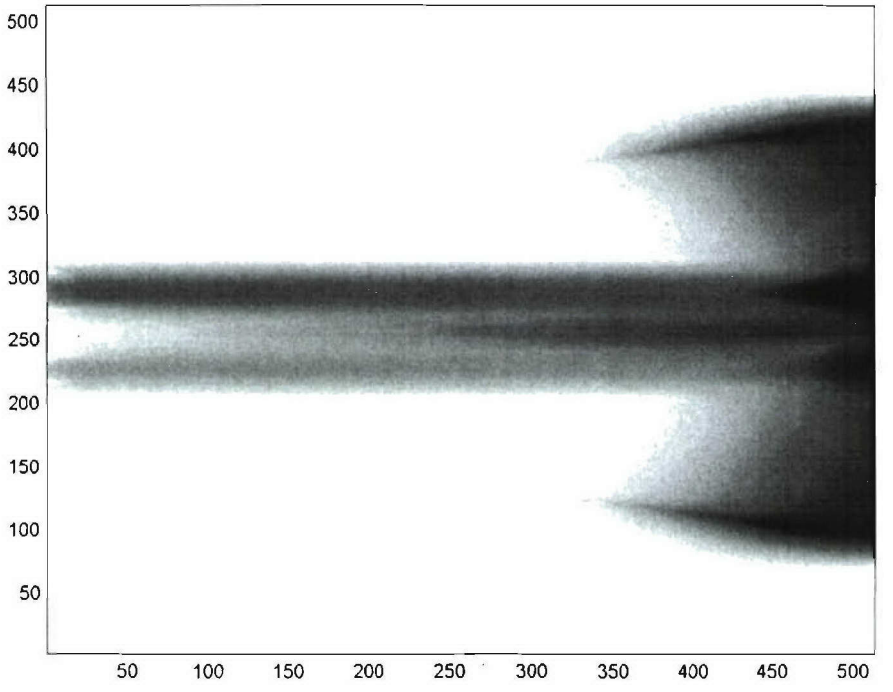

Figure A.8: *"Sorted" time-frequency representation*

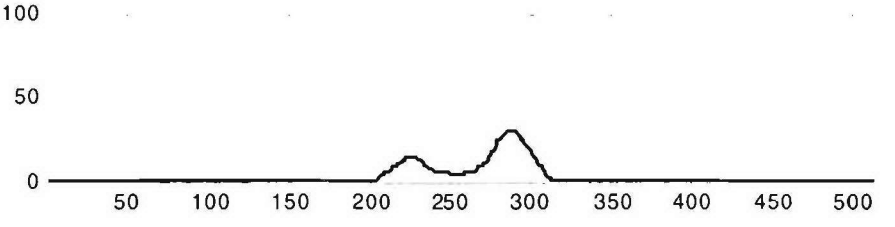

Figure A.9: *Statistics for the narrow window case (L1 smallest samples, L2 median samples, and L3 highest samples)*

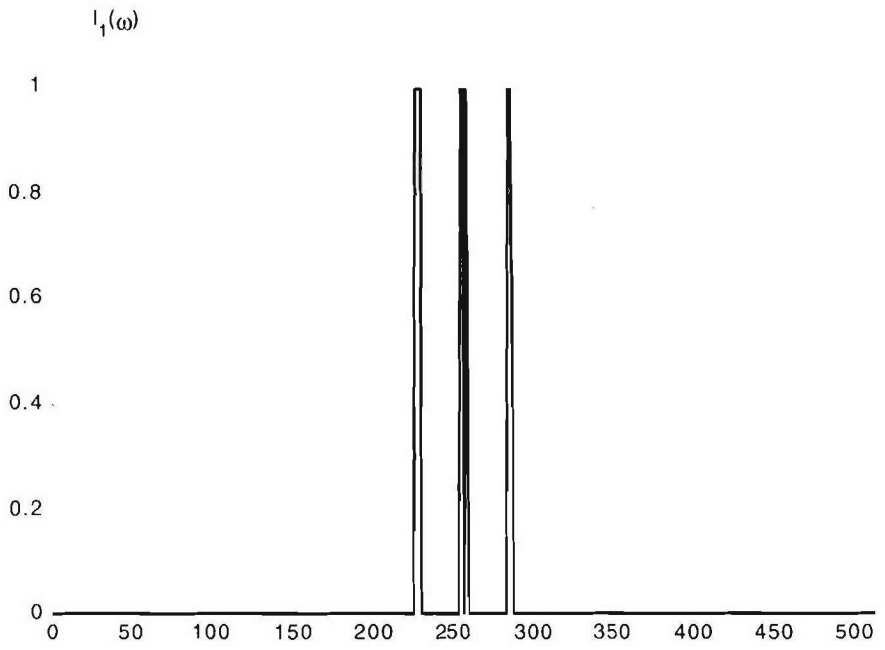

Figure A.10: *Indicator function for the stationary patterns (rigid body influence)*

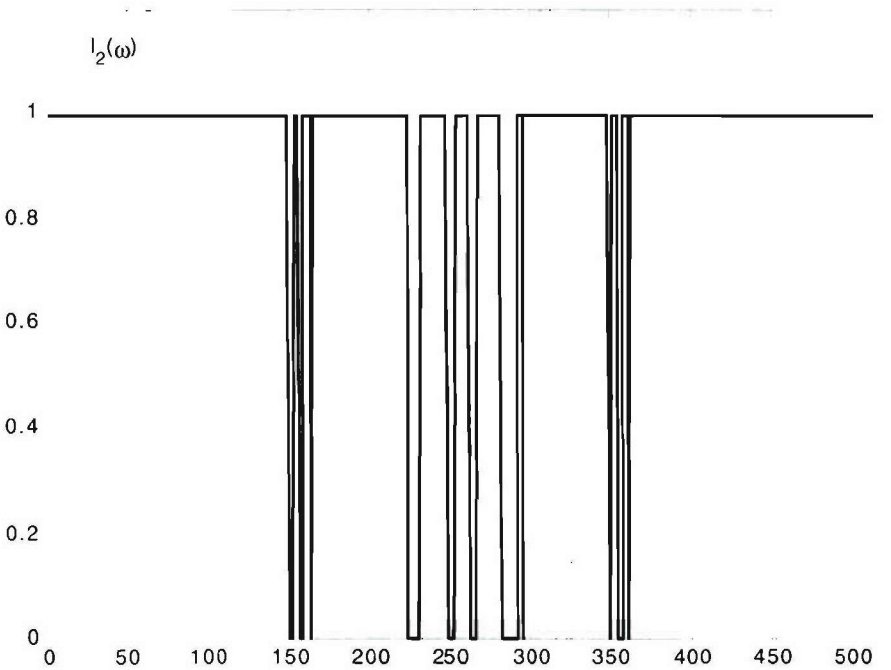

Figure A.11: *Indicator function for the sinusoidal FM signal pattern (rotating part influence)*

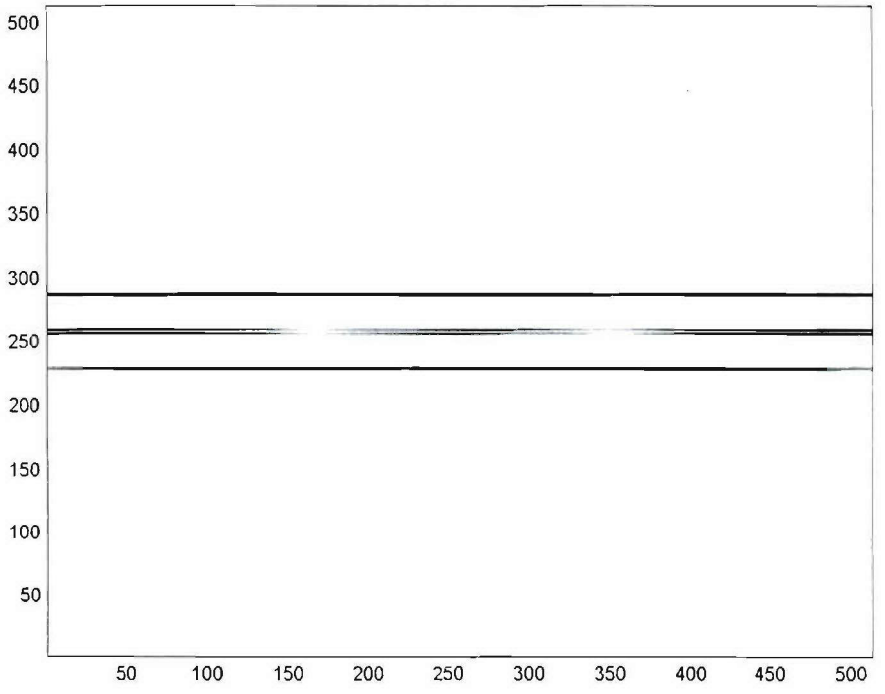

Figure A.12: *Detected stationary pattern (rigid body influence) after the proposed procedure*

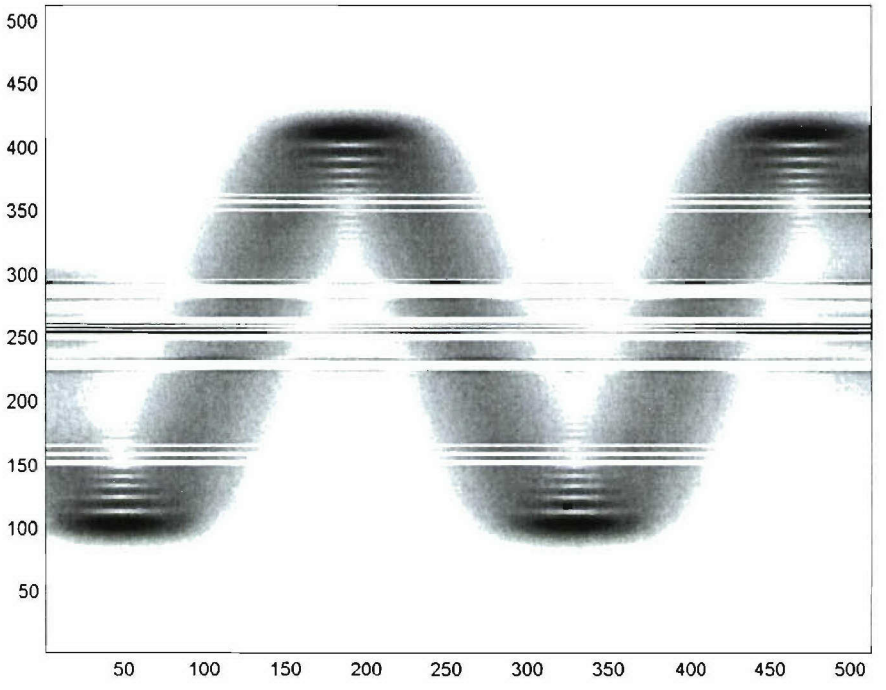

Figure A.13: *Detected sinusoidal FM signal (rotating part influence) after the proposed procedure*

References

1. T. Thayaparan, S. Abrol, and E. Riseborough: "Micro-Doppler feature extraction of experimental helicopter data using wavelet and time-frequency analysis," *RADAR 2004, Proc. of the International Conference on Radar Systems*, 2004.

2. T. Thayaparan, S. Abrol, V. C. Chen, and E. Riseborough: "Analysis of Micro-Doppler radar signatures from experimental helicopter and human data", NATO SET-80 symposium, Oslo, Norway, Oct. 2004.

3. J. Misiurewicz, K. Kulpa, and Z. Czekala: "Analysis of recorded helicopter echo", *IEE Radar 98, Proceedings*, pp. 449-453.

4. V. C. Chen, F. Li, S.-S. Ho, H. Wechsler: "Analysis of micro-Doppler signatures," *IEE Proc. Radar, Sonar, Navig.*, Vol. 150, No. 4, Aug. 2003, pp. 271-276.

5. V. C. Chen: "Micro-Doppler effect in radar: Part I: Phenomenon, physics, mathematics, and simulation study", *IEEE Trans. Aero. and El. Syst*, preprint.

6. T. Thayaparan and S. Abrol, Micro-Doppler Analysis of Rotating Target in SAR, DRDC Ottawa TM 2005-204, December 2005, 43 pages.

7. T. Thayaparan, S. Abrol, and E. Riseborough, Micro-Doppler radar signatures for intelligent target recognition, DRDC Ottawa TM 2004-170, 57 pages,

8. J. Li, H. Ling: "Application of adaptive chirplet representation for ISAR feature extraction from targets with rotating parts", *IEE Proc. Radar, Sonar, Navig.*, Vol.150, No.4, August 2003, pp.284-291.

9. T. Thayaparan, "Micro-Doppler analysis of the rotation antenna in airborne SAR image collected by the APY-6 radar," *IRS 2005*, Berlin, Germany, Sept. 2005.

10. W. J. Williams, E. J. Zalubas: "Invariant classification of time-frequency representations: Applications to Doppler radar target identification," in *Proc. of DSTO/DOD Workshop*, Adelaide, Austr. 1997.

11. P. Setlur, M. Amin, T. Thayaparan: "Micro-Doppler signal estimation for vibrating and rotating targets," in *Proc. of ISSPA 2005*, Sydney, Austr. 2005, pp. 639-642.

12. Y. Wang, H. Ling, and V. C. Chen, "ISAR motion compensation via adaptive joint time-frequency techniques," *IEEE Trans. Aerosp., Electron. Syst.*, Vol. 38, No. 2, 1998, pp. 670-677.

13. H. A. David, H. N. Nagaraja: Order statistics, Wiley, 2003.

14. F. Gini, G. B. Giannakis: "Hybrid FM-polynomial phase signal modeling: Parameter estimation and Cramer-Rao Bounds," *IEEE Trans. Signal Processing*, Vol. 47, No. 2, Feb. 2003, pp.363-377.

15. I. Pitas: *Digital image processing algorithms*, Prentice Hall 1993.

16. T. Thayaparan, G. Lampropoulos, S. K. Wong, and E. Risenborough: "Application of adaptive joint time-frequency algoritgm for focusing distorted ISAR images from simulated and measured radar data," *IEE Proc. Radar, Sonar, Navig.*, Vol. 150, No. 4, Aug. 2003, pp. 213-220.

17. T. Sparr and B. Krane: "Micro-Doppler analysis of vibrating targets in SAR," *IEE Proc. Radar Sonar Navig.*, Vol. 150, No. 4, Aug. 2003, pp. 277-283.

18. S. L. Marple: "Special time-frequency analysis of helicopter Doppler radar data", in *Time-Frequency Signal Analysis and Processing*, ed. B. Boashash, Elsevier 2004.

19. S. Wong, E. Riseborough, and G. Duff: "Experimental investigations on the distortion of ISAR images using different radar waveforms," Defence R&D Canada - Ottawa, DRDC Ottawa TM 2003-196, 2003.

20. S. Wong, E. Riseborough, and G. Duff: "Distortion in the ISAR (inverse synthetic aperture radar) images from moving targets," in *Proc. of IEEE ICIP*'2004, Vol. I, pp. 25-28, 2004.

21. L. Stanković, T. Thayaparan, and I. Djurović, "Time-Frequency Representation Based Approach for Separation of Target Rigid Body and Micro-Doppler Effects in ISAR Imaging," *IEEE Trans. Aero. and El. Syst*, preprint.

DOCUMENT CONTROL DATA

(Security classification of title, body of abstract and indexing annotation must be entered when the overall document is classified)

1. ORIGINATOR (the name and address of the organization preparing the document. Organizations for whom the document was prepared, e.g. Establishment sponsoring a contractor's report, or tasking agency, are entered in section 8.)

Defence R&D Canada – Ottawa
Ottawa, Ontario, Canada K1A 0Z4

2. SECURITY CLASSIFICATION (overall security classification of the document, including special warning terms if applicable)

UNCLASSIFIED

3. TITLE (the complete document title as indicated on the title page. Its classification should be indicated by the appropriate abbreviation (S,C or U) in parentheses after the title.)

Separation of target rigid body and micro-Doppler effects in ISAR/SAR imaging (U)

4. AUTHORS (Last name, first name, middle initial)

Thayaparan, Thayananthan

5. DATE OF PUBLICATION (month and year of publication of document)	6a. NO. OF PAGES (total containing information. Include Annexes, Appendices, etc.)	6b. NO. OF REFS (total cited in document)
September 2006	57	21

7. DESCRIPTIVE NOTES (the category of the document, e.g. technical report, technical note or memorandum. If appropriate, enter the type of report, e.g. interim, progress, summary, annual or final. Give the inclusive dates when a specific reporting period is covered.)

DRDC Ottawa Technical Memorandum

8. SPONSORING ACTIVITY (the name of the department project office or laboratory sponsoring the research and development. Include the address.)

Defence R&D Canada – Ottawa
Ottawa, Ontario, Canada K1A 0Z4

9a. PROJECT OR GRANT NO. (if appropriate, the applicable research and development project or grant number under which the document was written. Please specify whether project or grant)	9b. CONTRACT NO. (if appropriate, the applicable number under which the document was written)
15ec05	

10a. ORIGINATOR'S DOCUMENT NUMBER (the official document number by which the document is identified by the originating activity. This number must be unique to this document.)	10b. OTHER DOCUMENT NOS. (Any other numbers which may be assigned this document either by the originator or by the sponsor)
DRDC Ottawa TM 2006-187	

11. DOCUMENT AVAILABILITY (any limitations on further dissemination of the document, other than those imposed by security classification)

(X) Unlimited distribution
( ) Distribution limited to defence departments and defence contractors; further distribution only as approved
( ) Distribution limited to defence departments and Canadian defence contractors; further distribution only as approved
( ) Distribution limited to government departments and agencies; further distribution only as approved
( ) Distribution limited to defence departments; further distribution only as approved
( ) Other (please specify):

12. DOCUMENT ANNOUNCEMENT (any limitation to the bibliographic announcement of this document. This will normally correspond to the Document Availability (11). However, where further distribution (beyond the audience specified in 11) is possible, a wider announcement audience may be selected.)

13. ABSTRACT (a brief and factual summary of the document. It may also appear elsewhere in the body of the document itself. It is highly desirable that the abstract of classified documents be unclassified. Each paragraph of the abstract shall begin with an indication of the security classification of the information in the paragraph (unless the document itself is unclassified) represented as (S), (C), or (U). It is not necessary to include here abstracts in both official languages unless the text is bilingual).

(U) The micro-Doppler (m-D) effect is caused by moving parts of the radar target. This effect can degrade the quality of the ISAR/SAR image. However, at the same time, it carries information about the features of moving parts. The separation of the patterns caused by the stationary parts of the target from those caused by the moving (rotating or vibrating) parts is the topic of this report. Two techniques for the separation of the rigid part from the rotating parts have been proposed. The first technique is based on the time-frequency (TF) representation with sliding windows and order statistics techniques. The first step in this technique is the recognition of rigid parts in the range/cross-range plane. In the second step, the spectrogram and order statistics setup are employed to obtain the signals caused by the moving parts. The second technique based on the Radon transform can be applied in the case of very emphatic m-D effect. In the first step the rotating parts are recognized, based on the inverse Radon transform. After masking these patterns, a radar image with the rigid body reflection can be obtained. The proposed methods are illustrated by examples. The proposed methods not only focus the distorted SAR/ISAR images, but also provide additional information about the rotating/vibrating features of the target.

14. KEYWORDS, DESCRIPTORS or IDENTIFIERS (technically meaningful terms or short phrases that characterize a document and could be helpful in cataloguing the document. They should be selected so that no security classification is required. Identifiers such as equipment model designation, trade name, military project code name, geographic location may also be included. If possible keywords should be selected from a published thesaurus. e.g. Thesaurus of Engineering and Scientific Terms (TEST) and that thesaurus-identified. If it is not possible to select indexing terms which are Unclassified, the classification of each should be indicated as with the title.)

SAR
ISAR
Micro-Doppler
Micro-Motion
L-statistics
Time-Frequency Analysis
Moving Targets
Target Detection
Fourier Transform
Doppler Processing
Image Analysis
Radon Transform

Defence R&D Canada

Canada's Leader in Defence
and National Security
Science and Technology

R & D pour la défense Canada

Chef de file au Canada en matière
de science et de technologie pour
la défense et la sécurité nationale

www.drdc-rddc.gc.ca